



Thermodynamics, economic and environmental analyses of a hybrid waste–solar thermal power plant

A. Arabkoohsar¹ · M. Sadi¹

Received: 30 November 2019 / Accepted: 13 March 2020 / Published online: 2 April 2020
 © Akadémiai Kiadó, Budapest, Hungary 2020

Abstract

A novel hybrid configuration of solar parabolic trough collectors–waste incineration power plant was recently analyzed energetically in Denmark. Taking into account the true meaning of sustainability which is environmental friendliness and cost-effectiveness, and considering the existing gap of knowledge on the thermodynamic performance aspects of this hybrid system, this work conducts a thorough thermodynamic and sustainability analysis of this power plant. The main aim is to give a clear picture of the main advantages and any possible shortcomings of the hybrid power plant. For this purpose, the performance of the system is simulated for an entire year of operation under realistic solar irradiation fluctuations. The energy performance indices of the system are quantified and discussed. The exergy assessment of the hybrid cycle is accomplished, and the main sources of exergy destruction and economic losses are identified. The results show that the steam generator and the turbine cause the largest rates of irreversibilities of 36% and 20.8%. The environmental benefits and the overall cost of energy production of the system are calculated and compared to some other alternative power plants. In addition to the consistency of electricity production, the LCOE of the hybrid power plant decreases by 67% in comparison with the solar power plant. Comparing the system with a natural gas-fired power plant in terms of CO₂ emission, it is shown that the hybrid system leads to less 74.5 thousand tonnes of CO₂ emitted over an entire year.

Keywords Parabolic trough solar collector · Waste incineration · Thermodynamic and sustainability analysis · Dispatchable power · Performance improvement

List of symbols

A	Area (m ²)
D	Diameter (m)
$E_{\text{CO}_2\text{e}}$	Amount of CO ₂ e emission (–)
\dot{E}_{gen}	Electricity power (kW)
E_{λ}	Emission of different types of greenhouse gases (–)
Ex	Exergy (kW)
GWP_{λ}	Global warming potential of greenhouse gases (–)
h	Enthalpy (kJ kg ^{–1})
h_c	Convective heat transfer coefficient (kJ m ^{–2} K ^{–1})
$I\$_t$	Installation fees (\$)
IAM	Incidence angle modifier (–)
K	Thermal conductance (kJ m ^{–1} K ^{–1})

LHV	Low heat value (kJ kg ^{–1})
$M\$$	Maintenance fees (\$)
\dot{m}	Mass flow rate of the first preheating line (kg s ^{–1})
\dot{m}_{PTC}	Mass flow rate solar field (kg s ^{–1})
\dot{m}_s	Total mass flow rate of steam (kg s ^{–1})
Nu	Nusselt Number (–)
$O\$_t$	Operation fees (\$)
P	Pressure (kPa)
Pr	Prandtl number (–)
$q'_{12\text{Conv}}$	Convective heat transfer between SHTF and the absorber (kJ m ^{–1})
$q'_{23\text{Cond}}$	Conductive heat transfer through the absorber wall (kJ m ^{–1})
$q'_{34\text{Rad}}$	Heat transfer from the absorber to the glass envelope (kJ m ^{–1})
$q'_{3\text{SolAbs}}$	Solar Heat absorbed by the absorber (kJ m ^{–1})
$q'_{45\text{Cond}}$	Conductive heat transfer through the glass envelope (kJ m ^{–1})
$q'_{56\text{Conv}}$	Convective Heat transfer from the glass envelope to the atmosphere (kJ m ^{–1})

✉ M. Sadi
 ahm@et.aau.dk

¹ Department of Energy Technology, Aalborg University, Esbjerg, Denmark

$q'_{56\text{Rad}}$	Radiative Heat transfer from the glass envelope to the atmosphere (kJ m^{-1})	CT	Cooling Tower
$q'_{57\text{Rad}}$	Radiative Heat transfer from the glass envelope to the sky (kJ m^{-1})	De	Destruction
$q'_{5\text{SolAbs}}$	Solar absorption in the glass envelope (kJ m^{-1})	env	Envelope
q'_{cond}	Heat rejected in condenser (kJ kg^{-1})	FG	Flue gas
$q_{\text{Cond,bracket}}$	Conductive heat transfer through the bracket support (kJ m^{-1})	G	Generator
q'_{si}	Solar irradiation per receiver length (kJ m^{-1})	gen	Generation
\dot{Q}_{cond}	Rate of heat rejected in condenser (kW)	HC	Hybrid cycle
\dot{Q}_{WI}	Heat released in waste incineration process (kW)	HPT	High-pressure turbine
T	Temperature (K)	IPT	Intermittent pressure turbine
y	The flow rate of steam withdrawals form the first turbine (–)	LPT	Low-pressure turbine
y'	The flow rate of steam withdrawals form the second turbine (–)	MC	Mixing chamber
\dot{W}	Work production rate (kW)	MSW	Municipal solid waste
$\$_{\text{MSW}}$	Annual cost of the municipal waste (\$)	Net	Net
C, H, O, N, S	Mass fraction of carbon, hydrogen, oxygen, nitrogen and sulfur	OFWH	Open feed water heater
		opt	Optical
		P	Pump
		PH	Preheater
		PTC	Parabolic trough collector
		Rad	Radiation
		RC	Rankine cycle
		s	Steam
		SF	Solar fluid
		SG	Steam generator
		Sol	Solar
		ST	Steam turbine
		WI	Waste incineration

Greek symbols

α_{abs}	Absorptance of the absorber
α_{env}	Absorptance of the envelope
ε	Emissance
ε_x	Exergy efficiency
ε'_1	Shadowing factor
ε'_2	Tracking error
ε'_3	Geometry error (mirror alignment)
ε'_4	Dirt on mirrors
ε'_5	Dirt on collector
ε_6	Unaccounted factor
η	Efficiency
η_{abs}	Effective optical efficiency at absorber
η_{env}	Effective optical efficiency at the glass envelope
η_{gen}	Electricity generation efficiency
ξ	Exhaust gas volume
η_{WI}	Thermal efficiency of waste incineration plant
τ	Transmittance

Subscripts

A	Air
abs	Absorber
c	Cover
ci	Cover inner
CFWH	Closed feed water heater
ch	Chemical
conv	Convection

Introduction

A significantly higher share of renewable energy in the national energy systems is a serious aim of many countries which is, of course, much challenging in many aspects [1]. For example, the most popular renewable energy sources (solar and wind energy) are available on irregular profiles [2]. This is even of more importance for solar technologies as they are being used in a much wider range of applications in all the energy sectors including heating, cooling, power and even transportation [3]. Among the possible fluctuating energy stabilization methods, the use of energy storage systems and the hybridization of such systems with conventional energy production technologies might be considered as the two best solutions [4].

Energy storage technologies emerge as a response to synchronizing electricity supply and demand, thus enabling the electrical grid to be managed in a consistent manner [5]. Although heat storage technologies have mature state of the art making it quite easy and affordable to store renewable heat (including solar heat), the knowledge of electricity storage is still in the development phase. Apart from batteries that offer a high energy efficiency but yet suffer from the low energy density and high cost, there are a large number of mechanical/chemical energy storage

systems, such as flywheel storage [6], pumped hydropower storage [7], high-temperature heat and power storage [8], and compressed air energy storage [9] [10], each of which has its disadvantages, slowing down its deployment in the energy market.

Europe is pursuing an aggressive program to increase its share of renewable energy sources [11]. The combination of the intermittent renewable energy systems, specifically solar technologies, with conventional controllable energy production systems for delivering a stable energy output is also a broadly used and reliable measure [12]. Achour et al. [13] presented an analysis of a hybrid solar power plant in the south of Algeria via thermodynamic modeling and calculating the achievable solar-to-power efficiency from the hybrid plant. Liu et al. [14] investigated a novel hybrid cogeneration solar-exhaust heat power plant and calculated the total and electrical efficiencies of, respectively, 80.6% and 24.7%. Parisch et al. [15] suggested the hybridization of solar collectors and heat pumps (with the ground as the low-temperature heat source) and did an energy/exergy assessment of the system via developing the system model in TRANSYS. Khan et al. [16] presented a combined configuration, comprising solar systems with other sources/systems, for supplying the electricity of a Chinese island. Li et al. [17] offered a cascade power plant design in which a solar system and a natural gas-driven system are combined, concluded that the hybrid system offers a faster payback period than a solar Rankine cycle. A review of solar PVT collectors employed in cogeneration power plants was presented by Kasaeian et al. [18]. A system of energy combining solar collectors and fuel cells was presented for a Lebanese city [19], and it was concluded that the combinations of fuel cell-PV and fuel cell-solar thermal result in almost the same energy production level while the former will lead to a better minimum threshold power. Arabkoohsar and Andresen [20] proposed an intelligent hybrid design of solar-based cold production system and district heating supply for providing a hospital with stable profiles of cooling and heating.

Solar thermal power plants may come in various technologies including parabolic trough systems, linear Fresnel reflectors, solar dish/engine systems, and solar power towers [21]. Apart from the type of technology, all of the above-mentioned systems suffer from the intermittent source of energy. Thus, for the efficient performance of these technologies, either the use of an energy storage system or a hybridization with a secondary source of energy is vital. Hybrid concentrating solar power plants combined with different gas firing technologies [22], a solar thermal power plant combined with a geothermal power plant and a heat storage system [23], hybrid conventional fuel-solar electricity production plants [24], etc., are only a few of the many hybrid solar power systems studied before. A comprehensive review of various hybrid solar power systems with conventional

power technologies such as Brayton, Rankine, and the combined cycles is presented by Behar [25].

Waste incineration plants are quite common in many of the world's national energy systems today [26]. The main reasons for this are that not only incineration is a good method of disposal of municipal solid waste in environmental aspects but also releases much heat that might be utilized for power generation or heat supply for other applications [27]. Countries like Denmark and Germany are among those lands which take this business seriously to the extent that they import municipal solid wastes from other countries [28]. Munster and Meibom [29] analyzed the feasibility of further implementation of municipal solid waste incineration plants in the future in different countries of the world. Erikson et al. [30] investigated the technical performance of various waste firing energy production technologies when employed for supplying the demanding energy of district heating systems. Udono and Sitte [31] proposed and modeled a waste incineration-based plant for seawater desalination. Hedberg and Danielssen [32] studied the feasibility of waste firing driven absorption machines for supplying the demanding cooling energy of residential districts in Thailand.

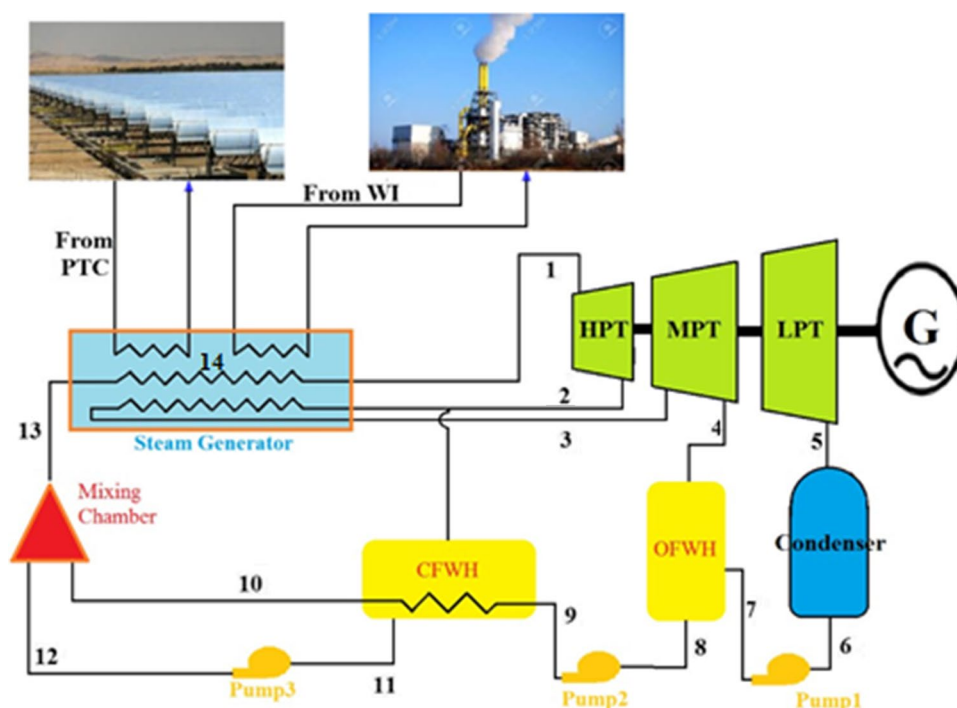
Recently, Sadi and Arabkoohsar [33, 34] proposed a hybrid configuration of solar parabolic trough collector (PTC)-waste incineration plant aiming at stabilizing the energy production of solar thermal power plants. In this hybrid solar–waste system, the waste firing unit comes as an auxiliary heat supply system for compensating the fluctuations of the available solar energy for the plant. In this way, the power plant could be managed to produce power at a certain desired level at any time of the day and the year. It was shown that by such integration, increased dispatchability, more reliability, and improved efficiency may be achieved. This study, as the supplement of the previous work, presents thorough sustainability and thermodynamic analysis of the hybrid PTC-waste incineration system to better address the pros and cons of the system and find the main energy and exergy loss/destruction points and reasons in the cycle. Based on the obtained results, a sort of recommendations for improving the energy and exergy efficiencies of the plant, and subsequently enhancing its economic index and environmental friendliness, are presented.

Hybrid solar–waste power plant

Figure 1 illustrates the configuration of the combined solar–waste firing power plant which comes with a Rankine-based power block.

As seen in the figure and as mentioned before, in this system, the waste incinerator is to be the auxiliary source of heat for the power plant which compensates for the

Fig. 1 The schematic of the hybrid power system, i.e., a Rankine cycle driven by a combined solar–waste heat source; CFWH: closed feedwater tank, OFWT: open feedwater tank, WI: waste incinerator



fluctuation of solar irradiation. Therefore, the solar thermal unit which is indeed a farm of LS2-PTC collectors is the primary source of the energy of the hybrid power plant. The heat supplied by the solar field and that provided by the waste incineration unit is given to the steam of the power block (a Rankine cycle) via the steam generator.

PTC is one of the common types of concentrating technologies for solar thermal power systems. Figure 2 represents the schematic of a PTC (upper panel), the cross-sectional view of its receiver (lower panel, left), and the grid of thermal resistance from the working fluid through the receiver (lower panel, right). There is very detailed information about how PTC panels operate in Ref. [33]. In addition, the NREL [32] has extensively modeled and experimentally analyzed the performance of such solar collectors and presented a comprehensive report which can be used as the reference of calculations and also a resource for the validation of mathematical and numerical models developed on PTCs.

Having detailed information about how solar collectors operate and how much energy the solar field can deliver at every moment, one can evaluate the heating duty of the waste incinerator. For simulating the process of incineration in the waste incinerator chamber, a specific municipal solid waste mixture is considered based on which the heating value of the waste is also calculated. The waste incineration process is assumed to take place in an incineration chamber (with waste source and a huge amount of air as the inputs), and the outputs of the chamber will be ash (almost one-sixth of the waste mass) and hot flue gas flow. With 80% excess air in the incineration process [36], the calculations give the

flue gas temperature of 1367 K at the chamber outlet. The design of the second part of the steam generator (the part associated with delivering waste firing unit energy to the power block) is so that the flue gas at the boiler exhaust will be at 483 K [37].

The power block of the system is a Rankine cycle with three turbine stages which is broadly in use in many real power plants all around the world. As the Rankine power cycle is a well-known technology and there is quite mature literature for that, no more elaboration on the details of the operation of such a plant is presented here.

Table 1 details the features of the PTCs used in the simulations of this work (i.e., the module of the LS-2 parabolic PTCs which is broadly referenced in the literature [38]), the waste incinerator unit [36] and the power block of the hybrid power plant [39].

It bears mentioning that the sizing of the power plant has been somewhat random because there is no specific case study with a solid load profile for the study. Thus, just as a random yet reasonable value, the solar thermal unit is sized for a nominal capacity of 15 MW electricity output of the power block. Regarding the waste incineration unit, in order to not fall way below the optimal operating conditions, the operation of the unit is so planned that its load never falls below 25% of its nominal capacity. In addition, for maximizing the solar field's heat supply share in the hybrid plant, the waste incineration unit will operate at the minimum level by the time of peak solar irradiation availability. Having said this, the waste incineration unit is sized as 20 MW at full capacity.

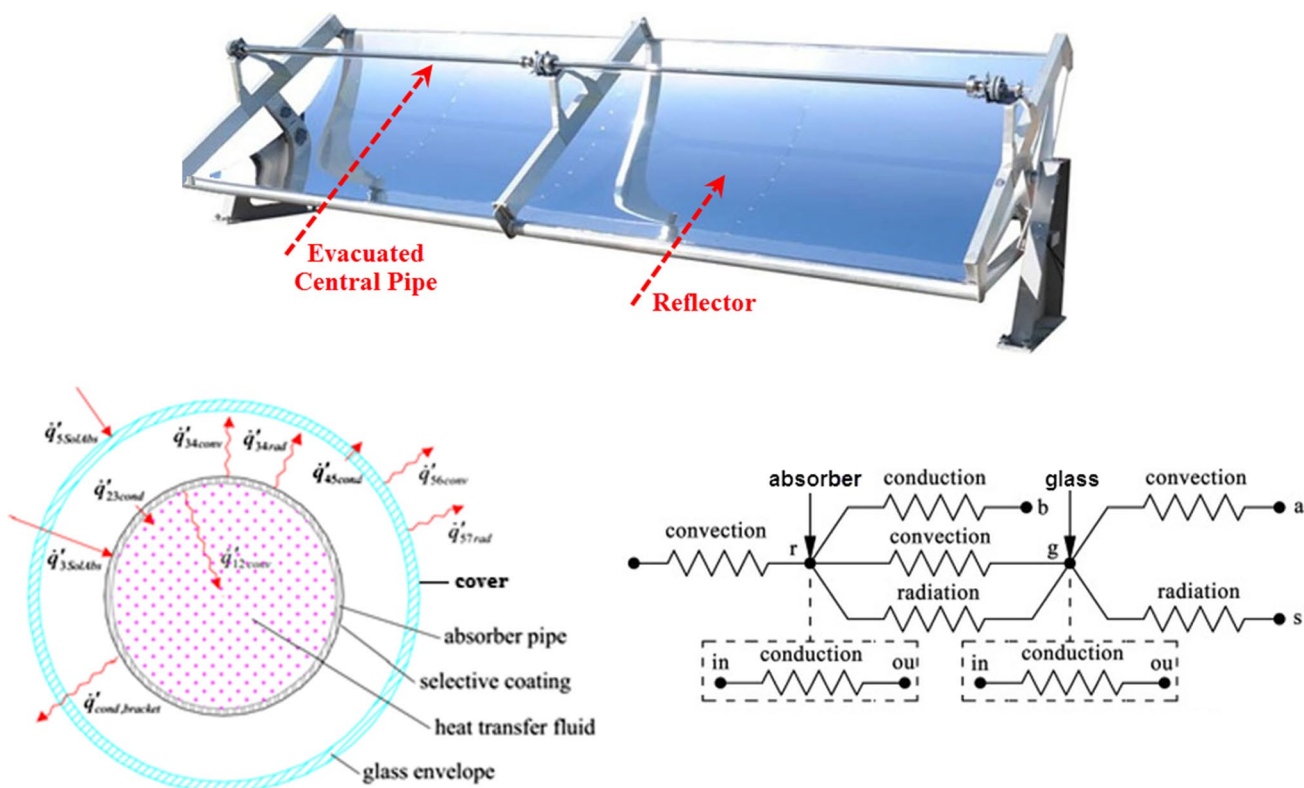


Fig. 2 The schematic of a PTC (up), its central pipe (down-left); and its thermal resistance circuit (down-right) [35]

Mathematical model

The mathematical model of the hybrid power plant is presented in four different parts of energy, exergy, economic and environmental modeling.

Energy model

There is a comprehensive energy model of this hybrid system in [33]. Therefore, a brief energy model of the hybrid power plant is given here.

For the power plant, the overall energy efficiency is defined as the rate of the amount of electricity generated by the generator (\dot{E}_G) divided by the rate of input energy, which is the summation of the solar energy irradiated to the collectors' field (\dot{I}_{Sol}) and the energy input of the waste incineration unit (LHV_{WI}) [33]:

$$\eta_{HC} = \frac{\dot{E}_{out}}{\dot{E}_{in}} = \frac{\dot{E}_G}{\dot{I}_{Sol} + LHV_{WI}} \tag{1}$$

In the Rankine cycle, the amount of producible power is the summation of the work produced by the three high-pressure, medium-pressure and low-pressure turbines minus the work

consumed by the pumps multiplied by the efficiency of the generator; thus, one can write [33]:

$$\dot{W}_{net} = \dot{E}_G / \eta_G; \text{ where } : \dot{W}_{net} = \dot{W}_{HPT} + \dot{W}_{IPT} + \dot{W}_{LPT} - \sum \dot{W}_P \tag{2}$$

With present pressure and temperature values at different points of the cycle, the steam flow rate through the cycle (\dot{m}_S) can be calculated by [33]:

$$\begin{aligned} \dot{W}_{net} = & \dot{m}_S w_{HPT} + (\dot{m}_S - \dot{m}_{PH1}) w_{IPT,I} \\ & + (\dot{m}_S - \dot{m}_{PH1} - \dot{m}_{PH2}) (w_{IPT,II} + w_{LPT}) \\ & - \dot{m}_S \sum w_P \end{aligned} \tag{3}$$

where w represents the specific work of turbomachinery in the cycle, \dot{m} is mass flow rate and the subscript PH refers to the preheating lines.

Denoting y and y' for the flow rate of steam withdrawals for the first and second preheaters, the energy balance of the condenser will be as below:

$$\dot{Q}_C = \dot{m}_S [(1 - y - y') (h_5 - h_6)] \tag{4}$$

The mass and energy balance equations for the steam generator will be as [33]:

Table 1 The characteristics of the PTCs, waste incinerator and the power block

Unit	Parameter	Value	
Solar collectors	PTC's width/length	5/7.8 m	
	PTC's focal distance	1.71 m	
	Area of the aperture of the PTC	39.0 m ²	
	The concentration ratio of the PTC	22.74	
	Inner/outer diameter of the receiver	66/70 cm	
	Inner/outer diameter of the cover	109/115 cm	
	Receiver/cover emittance factor	0.2/0.95	
	Absorbance factor of the absorber tube	0.96	
	Reflectance factor of the concentrator	0.83	
	Intercept factor	0.99	
	Waste Incineration	Type of waste	Municipal solid waste
		Mass proportion of the compositions	5.91% Ash
			47.18% Carbon
			6.25% Hydrogen
39.57% Oxygen			
0.91% Nitrogen			
0.18% Sulfur			
Heating value of waste		12,500 kJ kg ⁻¹	
Percentage of excess air		80%	
Temperature of combustion products		1376 K	
Temperature of flue gas	438 K		
Power Block	Heat transfer working flow	Industrial oil	
	Maximum production capacity	20 MW	
	Minimum operation level	5 MW	
	Nominal capacity	20 MW	
	Working fluid	Steam/water	
	Inlet temperature of the high-pressure turbine	500 °C	
	Inlet temperature of the medium-pressure turbine	500 °C	
	Inlet temperature of the low-pressure turbine	350 °C	
	Inlet pressure of the high-pressure turbine	10 MPa	
	Inlet pressure of the medium-pressure turbine	3 MPa	
Inlet pressure of the low-pressure turbine	0.25 MPa		
Condenser pressure	10 kPa		
Isentropic efficiency of turbines	85%		
Isentropic efficiency of pumps	85%		
Energy conversion efficiency of the generator	95%		

$$\dot{m}_{\text{PTC}} \cdot \Delta h_{\text{PTC}} = \dot{m}_S (h_{14} - h_{13}) \quad (5)$$

$$\dot{m}_{\text{FG}} \cdot \Delta h_{\text{FG}} = \dot{m}_S (h_1 - h_{13}) + \dot{m}_S (1 - y) (h_3 - h_2) \quad (6)$$

where the subscripts PTC and FG represent the PTC and the flue gas flow after the incineration chamber, respectively.

The energy equation for the open and closed feedwater tanks, as well as the mixing chamber, can simply be written based on the first law of thermodynamics. In order for fulfilling the above-presented modeling, one needs the model of the heat supply components, i.e., the solar collectors and the incineration process.

Regarding the PTCs, considering the heat flow diagram and the thermal resistances given in Fig. 2, one may write [33]:

$$\dot{q}'_{12\text{Conv}} = \dot{q}'_{23\text{Cond}} \quad (7)$$

$$\dot{q}'_{3\text{SolAbs}} = \dot{q}'_{34\text{Conv}} + \dot{q}'_{34\text{Rad}} + \dot{q}'_{23\text{Cond}} + \dot{q}'_{\text{Cond,bracket}} \quad (8)$$

$$\dot{q}'_{34\text{Conv}} + \dot{q}'_{34\text{Rad}} = \dot{q}'_{45\text{Cond}} \quad (9)$$

$$q'_{45\text{Cond}} + q'_{5\text{SolAbs}} = q'_{56\text{Conv}} + q'_{57\text{Rad}} \tag{10}$$

$$q'_{\text{HeatLoss}} = q'_{56\text{Conv}} + q'_{57\text{Rad}} + q'_{\text{Cond,bracket}} \tag{11}$$

The terms defined in the above equations are all the heat transfer flows indicated in Fig. 2 and also mentioned in the nomenclature of the article. A detailed formulation of these parameters can be found in [40]. These parameters are also formulated briefly here.

For $q'_{12\text{Conv}}$, as a convection heat exchange flow, one has [33]:

$$q'_{12\text{Conv}} = h_{c1} D_2 \pi (T_2 - T_1) \tag{12}$$

$q'_{23\text{Cond}}$ is conduction through the absorber pipe and is formulated as [33]:

$$q'_{23\text{Cond}} = 2\pi k_{\text{abs}} (T_2 - T_3) / \ln(D_3 - D_2) \tag{13}$$

$q'_{34\text{Rad}}$ is the heat radiation from the absorber and can be calculated by [33]:

$$q'_{34\text{Rad}} = \frac{\sigma \pi D_3 (T_3^4 - T_4^4)}{(1/\epsilon_3 + (1 - \epsilon_4) D_3 / (\epsilon_4 D_4))} \tag{14}$$

To calculate $q'_{45\text{Cond}}$, as the thermal conduction through the envelope, the air thermal conductance of Pyrex glass envelope is considered 1.04 W m^{-2} [41].

$q'_{56\text{Conv}}$ is the convective heat losses from the cover to the ambient and might be calculated by [40]:

$$q'_{56\text{Conv}} = h_{\text{conv-out}} D_5 \pi (T_5 - T_6) \tag{15}$$

$$h_{\text{conv-out}} = \frac{k_{56} \text{Nu}_{D5}}{D_5} \tag{16}$$

$$\text{Nu}_{D5} = C \text{Re}_{D5}^m \text{Pr}_6^n \left(\frac{\text{Pr}_6}{\text{Pr}_5} \right)^{1/4} \tag{17}$$

Irradiation from the envelope, i.e., $q'_{57\text{Rad}}$, is given by [33]:

$$q'_{57\text{Rad}} = \sigma \pi D_5 \epsilon_5 (T_5^4 - T_7^4) \tag{18}$$

Here T_7 is effective sky temperature (K) and ϵ_5 is the emittance factor of the envelope.

The incoming solar radiation from the reflector to the receiver is absorbed by the envelope (i.e., $q'_{5\text{SolAbs}}$) and the absorber ($q'_{3\text{SolAbs}}$). These parameters are defined as below [33]:

$$q'_{\text{glass - Abs}} = q'_{\text{si}} \epsilon'_1 \epsilon'_2 \epsilon'_3 \epsilon'_4 \epsilon'_5 \epsilon'_6 \rho_{\text{cl}} \text{IAM} \cdot \alpha_{\text{env}} \tag{19}$$

$$q'_{\text{absorber-Abs}} = q'_{\text{si}} \eta_{\text{env}} \tau_{\text{env}} \alpha_{\text{abs}} \tag{20}$$

in which q'_{si} and α_{env} are solar energy radiated on a unit length of the receiver, and the absorptance factor of the glass envelope. The term IAM represents the incidence angle modifier, α_{abs} is the absorptance factor of the absorber, and τ_{env} is the glass envelope transmittance factor.

With respect to the incineration process, the following equations as the mass and energy balance equations on the incinerator chamber are used [42]:

$$\dot{m}_A + \dot{m}_{\text{MSW}} = \dot{m}_{\text{Ash}} + \dot{m}_{\text{FG}} \tag{21}$$

$$\dot{m}_A \bar{h}_A + \sum_j \dot{m}_j \bar{h}_j = \dot{m}_{\text{Ash}} \bar{h}_{\text{Ash}} + \sum_k \dot{m}_k \bar{h}_k \tag{22}$$

where the subscripts *A*, *MSW* and *Ash* stand for the airflow and the waste injected to and the ash discharged from the chamber. Also, *j* and *k* are the counters of the components of the waste and flue gas mixtures, respectively. Note that \bar{h} refers to the total enthalpy including the physical and chemical enthalpies of the components.

Exergy model

Before presenting a detailed exergy model of the hybrid system, a short explanation of the fundamentals of exergy analysis is given. Exergy (EX) is technically defined as the maximum work production potential of an entity, e.g., a fluid stream, etc., due to the different conditions it has compared to the dead state, i.e., the thermodynamic equilibrium of the entity with the environment.

By the same token as the previous section, the exergy model of the hybrid system comes in the four subsections of the whole system model, the Rankine cycle exergy model, the model of the solar collector module, and the model of an incineration process.

The hybrid system The rate of exergy input of the power plant is the summation of the exergy of the waste material supplied ($\dot{E}X_{\text{WI}}$) and the incoming solar exergy ($\dot{E}X_{\text{Sol}}$). This can be written mathematically as below:

$$\dot{E}X_{\text{in}} = \dot{E}X_{\text{WI}} + \dot{E}X_{\text{Sol}} \tag{26}$$

The net exergy output of the system is equal to the rate of power produced at each time step (\dot{E}_G). The overall exergy efficiency of the whole hybrid system (ϵ_{HC}) can then be given by [43]:

$$\epsilon_{\text{HC}} = \frac{\dot{E}_{\text{gen}}}{\dot{E}X_{\text{SLR}} + \dot{E}X_{\text{WI}}} \tag{27}$$

The Rankine cycle The net exergy output of the hybrid system is directly a function of the exergy efficiency of the

components of the Rankine cycle. By calculating the rate of exergy destruction through/by a component, and having the rate of exergy input of that, one could easily assess the exergy performance of the given component. For this, one can write [43]:

$$\epsilon_i = \frac{\dot{E}X_{out}}{\dot{E}X_{in}} = \frac{\dot{E}X_{in} - \dot{E}X_i^{De}}{\dot{E}X_{in}} \tag{28}$$

where ϵ_i is the exergy efficiency of component i and $\dot{E}X_i^{De}$ is the rate of exergy destruction of the component.

Having said this, the rate of exergy destruction of the two-stage boiler, so-called steam generator, ($\dot{E}X_{SG}^{De}$), can be given by [43]:

$$\begin{aligned} \dot{E}X_{SG}^{De} &= \sum \dot{E}X_{in} - \sum \dot{E}X_{out} \\ &= (\dot{E}X_{13} + \dot{E}X_2 + \dot{E}X_{SF,in} + \dot{E}X_{WL,in}) \\ &\quad - (\dot{E}X_1 + \dot{E}X_3 + \dot{E}X_{SF,out} + \dot{E}X_{WL,out}) \end{aligned} \tag{29}$$

in which $\dot{E}X_{13}$, $\dot{E}X_2$, $\dot{E}X_{SF,in}$ and $\dot{E}X_{WL,in}$ are the exergy of streams 13 and 2, the exergy of the solar working fluid entering the steam generator and the inlet exergy of the waste incineration unit, respectively. As such, the terms $\dot{E}X_1$, $\dot{E}X_3$, $\dot{E}X_{SF,out}$ and $\dot{E}X_{WL,out}$ represent by turning the exergy of streams 1 and 3; the exergy of the solar fluid and the flue gas exits from the steam generator.

For the triple-stage turbine, the rate of exergy destruction ($\dot{E}X_{ST}^{De}$) can be given as below [43]:

$$\dot{E}X_{ST}^{De} = (\dot{E}X_1 + \dot{E}X_3) - (\dot{E}X_2 + \dot{E}X_4 + \dot{E}X_5) - \dot{W}_{ST} \tag{30}$$

in which the terms $\dot{E}X_1$, $\dot{E}X_2$, $\dot{E}X_3$, $\dot{E}X_4$ and $\dot{E}X_5$ are exergy of streams 1, 2, 3, 4 and 5 and \dot{W}_{ST} is produced work of steam turbine, respectively. Note that a model of the entire turbine set is given here while one may have the assessment of each stage of the turbine in terms of exergy performance as well.

The next main component of the power cycle is the condenser, for which the exergy destruction rate is given by [43]:

$$\dot{E}X_C^{De} = (\dot{E}X_{in} - \dot{E}X_{out})_S - (\dot{E}X_{out} - \dot{E}X_{in})_{CT} \tag{31}$$

where the subscripts S and CT stand for the steam flow and the cooling tower, respectively. The exergy efficiency of the condenser is calculated as:

$$\epsilon_{Cnd} = \frac{(\dot{E}X_{in} - \dot{E}X_{out})_S}{(\dot{E}X_{out} - \dot{E}X_{in})_{CT}} \tag{32}$$

Similarly, for the pump, one has [43]:

$$\dot{E}X_P^{De} = \dot{E}X_{in} - \dot{E}X_{out} + \dot{W}_P; \text{ and } : \epsilon_P = \frac{(\dot{E}X_{out} - \dot{E}X_{in})}{\dot{W}_P} \tag{33}$$

In a similar manner, one may have the following formulations for the open and closed feedwater tanks and the mixing chamber, respectively [43]:

$$\dot{E}X_{OFWH}^{De} = \dot{E}X_4 + \dot{E}X_7 - \dot{E}X_8; \text{ and } : \epsilon_{OFWH} = \frac{\dot{E}X_8}{\dot{E}X_4 + \dot{E}X_7} \tag{34}$$

$$\dot{E}X_{CFWH}^{De} = \dot{E}X_2 + \dot{E}X_9 - \dot{E}X_{10} - \dot{E}X_{11}; \text{ and } : \epsilon_{CFWH} = \frac{\dot{E}X_{10} - \dot{E}X_9}{\dot{E}X_2 - \dot{E}X_{11}} \tag{35}$$

$$\dot{E}X_{MC}^{De} = \dot{E}X_{10} + \dot{E}X_{12} - \dot{E}X_{13}; \text{ and } : \epsilon_{MC} = \frac{\dot{E}X_{13}}{\dot{E}X_{10} + \dot{E}X_{12}} \tag{36}$$

where the parameters $\dot{E}X_z$ are the exergy of the points z through the power plant (the points numbers can be seen in the configuration of the plant). $\dot{E}X_{OFWH}^{De}$, $\dot{E}X_{CFWH}^{De}$ and $\dot{E}X_{MC}^{De}$ are the exergy destruction of the open and closed feedwater tanks and the mixing chamber.

LS2 PTC For a PTC, the input exergy can be given by [44]:

$$\dot{E}X_{in,PTC} = I_b A_a \left(1 - \frac{4T_o}{3T_{sun}} (1 - \cos\delta)^{0.25} + \frac{1}{3} \left(\frac{T_o}{T_{sun}} \right)^4 \right) \tag{37}$$

in which T_o and T_{sun} are the dead state temperature and the sun's surface temperature (both in K), respectively. Here, the exergy efficiency is defined as the ratio of the net exergy gain to that received by the collector [44]:

$$\epsilon_{PTC} = \frac{\dot{E}X_{gain,PTC}}{\dot{E}X_{in,PTC}} = \frac{I_b A_a \left(1 - \frac{4T_o}{3T_{sun}} (1 - \cos\delta)^{0.25} + \frac{1}{3} \left(\frac{T_o}{T_{sun}} \right)^4 \right) - \dot{E}X_{PTC}^{De} - \dot{E}X_{PTC}^{Loss}}{I_b A_a \left(1 - \frac{4T_o}{3T_{sun}} (1 - \cos\delta)^{0.25} + \frac{1}{3} \left(\frac{T_o}{T_{sun}} \right)^4 \right)} \tag{38}$$

Note that exergy losses ($\dot{E}X_{PTC}^{Loss}$) are caused by optical error and heat transfer losses from the solar receiver and the exergy destruction ($\dot{E}X_{PTC}^{De}$) is due to heat transfer between the absorber and the solar working fluid. By introducing the dimensionless exergy term of $\dot{E}X' = \frac{\dot{E}X}{\dot{E}X_{in,PTC}}$, the exergy efficiency of the solar collectors may be defined as [45]:

$$\epsilon_{PTC} = 1 - \left(\dot{E}X'_{d,\Delta P} + \dot{E}X'_{d,q1} + \dot{E}X'_{d,q2} + \dot{E}X'_{loss,opt} + \dot{E}X'_{loss,q} \right) \tag{39}$$

where

$$\dot{E}X'_{d,q1} = \eta_o \left(1 + \frac{I_b A_a}{\dot{E}X_{in,PTC}} \left(\frac{\Delta z}{L_c} \sum_j \frac{T_o}{T_{aj}} - 1 \right) \right) \tag{40}$$

$$\dot{E}X'_{d,q2} = T_o \dot{m}_f \frac{\left(\int_{T_i}^{T_c} c_p(T) \frac{dT}{T} - \sum_j \frac{1}{T_{aj}} \int_{T_{ij}}^{T_{ej}} c_p(T) dT \right)}{\dot{E}X_{in,PTC}} \tag{41}$$

$$\dot{E}X'_{loss,opt} = 1 - \eta_o \tag{42}$$

$$\dot{E}X'_{loss,q} = \frac{\sum_j \dot{Q}_{j,loss} \left(1 - \frac{T_o}{T_{aj}} \right)}{I_b A_a \left(1 - \frac{4T_o}{3T_{sun}} (1 - \cos\delta)^{0.25} + \frac{1}{3} \left(\frac{T_o}{T_{sun}} \right)^4 \right)} \tag{43}$$

It should be noted that exergy destruction due to the friction of the viscous solar working fluid is not considered here.

Waste incineration For a waste incineration process, the rate of exergy destruction is given by [46]:

$$\dot{E}X_{W1}^{De} = \dot{E}X_{MSW} + \dot{E}X_A - \dot{E}X_{FG} - \dot{E}X_{Ash} \tag{44}$$

in which $\dot{E}X_{MSW}$, $\dot{E}X_A$, $\dot{E}X_{FG}$ and $\dot{E}X_{Ash}$ are the exergy of the waste burnt in the incineration process, the exergy of air consumed during the incineration process, the exergy of the flue gas produced and the exergy of the ash withdrawn from the incinerator chamber, respectively.

The exergy of the municipal waste can be calculated by [37]:

$$\dot{E}X_{MSW} = \dot{m}_{MSW} \left(1812.5 + 295.606C + 587.354H + 17.506O + 17.735N + 95.615S - 31.8Ash \right) \tag{45}$$

where the parameters C, H, O, N, S, and Ash are the mass of compositions carbon, hydrogen, oxygen, nitrogen, sulfur and ash, respectively.

The exergy of the ash can also be given as [46]:

$$\dot{E}X_A = \dot{m}_A \left(0.0004056T_{Ash}^2 + 0.01057T_{Ash} - 54.44 \right) \tag{46}$$

in which T_{Ash} is the temperature of the ash in K. The exergy rate of the flue gas supplied for Boiler 2, considering a perfect gas model for that, is calculated by the following equation [46]:

$$\dot{E}X_{FG} = \dot{m}_{FG} \left(\dot{E}X_{FG}^{ch} + c_{p,FG} (T_{FG} - T_o) - T_o \left(c_{p,FG} \ln \left(\frac{T_{FG}}{T_o} \right) - R \ln \left(\frac{P_{FG}}{P_o} \right) \right) \right) \tag{47}$$

here \dot{m}_{FG} , $\dot{E}X_{FG}^{ch}$, T_{FG} and P_{FG} refer to the mass flow rate, chemical exergy, temperature and pressure of the flue gas stream going out of the incineration chamber.

Note that since air enters the chamber in ambient temperature, the exergy of the airflow is to be zero.

Emission model

In the hybrid system proposed, naturally, the solar part is 100% environmentally friendly and it is the waste incineration unit that has an environmental impact. However, one should note that although the waste incineration process makes pollution, it prevents much more greenhouse gas from being emitted from the landfilling process of the municipal solid waste. The US environmental protection agency has measured how much emission is caused on average by municipal solid wastes when being incinerated or when being landfilled, resulting in 415 kg and 840 kg of CO₂e per tonne of waste [47]. Thus, incineration is an environmentally friendly process as it is preventing about 425 kg CO₂e per tonne of waste on average. This can also be mathematically calculated for any specific type of waste source by [48]:

$$E_{CO2e} = \sum E_{\lambda} GWP_{\lambda}; \text{where } : E_{\lambda} = \sum \mu_{\lambda} \xi M \tag{48}$$

where E_{λ} and GWP_{λ} are the amounts of emitted gas in the gas mixtures released in the environment from the chimney of the incinerator, and the global warming potential of each of these gases. Also, μ_{λ} , M and ξ are the emission concentration of each gas, the mass of the waste and the volume of exhaust gas mixture.

Economic model

The objective of this work for presenting an economic analysis of the system is to prove the feasibility of the hybridization proposed economically. Therefore, as a reliable index, the levelized cost of energy (LCOE) of the system is to be calculated and then compared to a number of popular power plant technologies, e.g., natural gas-based steam power

plant, gas turbine, combined cycle plant, pure solar energy plant, and pure waste incineration plant. The LCOE of an energy production system is calculated as [49]:

$$LCOE = \frac{\sum_{y=1}^Y \left[\frac{(I\$_t + M\$_t + O\$_t)}{(1+r)^y} \right]_y}{\sum_{y=1}^Y \left[\frac{(P)}{(1+r)^y} \right]_y}; \tag{49}$$

where : $\begin{cases} I\$_t = I\$_{Sol} + I\$_{WI} + I\$_{RC} \\ M\$_t = M\$_{Sol} + M\$_{WI} + M\$_{RC} \\ O\$_t = \$_{MSW} \end{cases}$

where $I\$$, $M\$$, and $O\$$ are, respectively, the capital (including the installation fees), the maintenance, and operation costs, while P is the amount of the power generation in a year. Also, r represents the interest rate, y and Y are the year number and the system’s lifetime (considered as 25 years). The item $\$_{MSW}$ is the annual cost of the municipal waste burnt in the system. The subscripts Sol, WIU and RC are, respectively, the solar system, the waste incineration unit and the Rankine cycle.

Results and discussion

In the results section, first of all, some information about the case study of this work, i.e., Aarhus city of Denmark, is given. Then, the model used for the PTC is validated. Afterward, the results of the energy, exergy, economic and environmental assessments are presented.

The case study information

The hybrid solar–waste-driven power plant is proposed to be built up in Aarhus, where there are several waste incineration units and the municipality together with the energy planers has decided to bring a solar thermal power plant into the energy system of the city. Figure 3 shows a duration curve of the solar energy availability in Aarhus on a horizontal surface in $W\ m^{-2}$. This figure shows that out of a total of 8760 h a year, only half of that offers solar irradiation and during about 1500 h; a solar irradiation intensity greater than $300\ W\ m^{-2}$ may be expected. A maximum of just below $900\ W\ m^{-2}$ can also be received by a horizontal surface in Aarhus mid-summer.

As mentioned before, the solar farm is supposed to hire tracking systems; thus, it is important to know how much solar energy is available for the tracking PTCs. Figure 4 makes a comparison of the amount of receivable solar radiation with a horizontal collector and a tracking collector during four typical seasonal days. This figure clearly shows the impact of the hiring tracking system, showing the big difference between fixed and tracking solar fields. This effect is even more during the summer as in this season a better solar energy collection index will result in a bigger difference.

Figure 5 shows the potential of Aarhus in terms of waste incineration capacity during 2015 in a total daily format. As seen, by 2015, there has existed a maximum of 85 MWh per day heat production capacity by waste incineration plants in the case study. The incineration units are mainly for the baseload supply of the local district heating system, which naturally decreases during the summer.

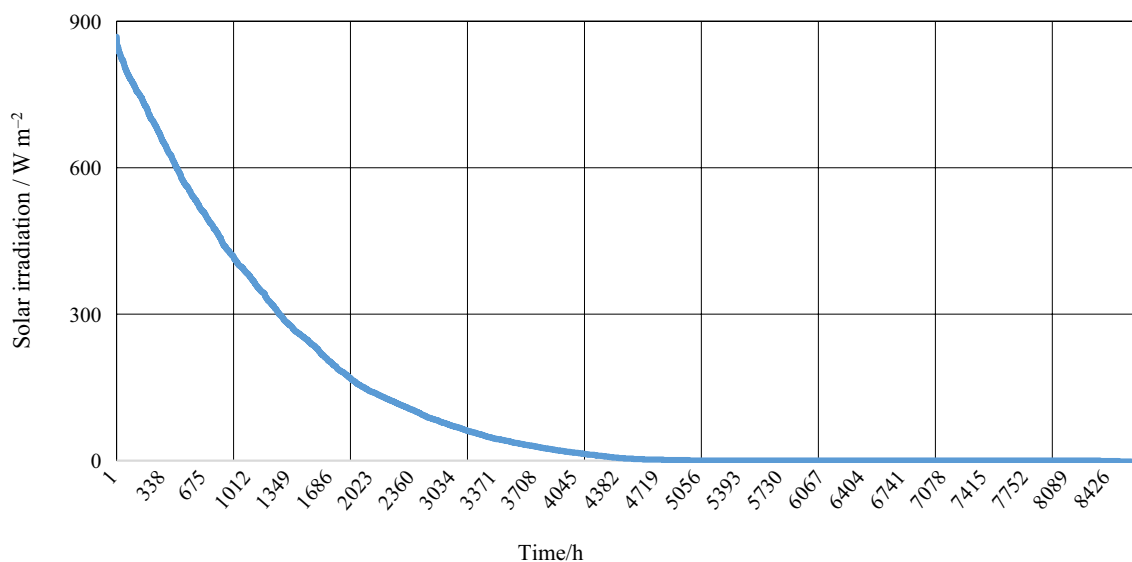


Fig. 3 Duration curve of solar irradiation in the case study

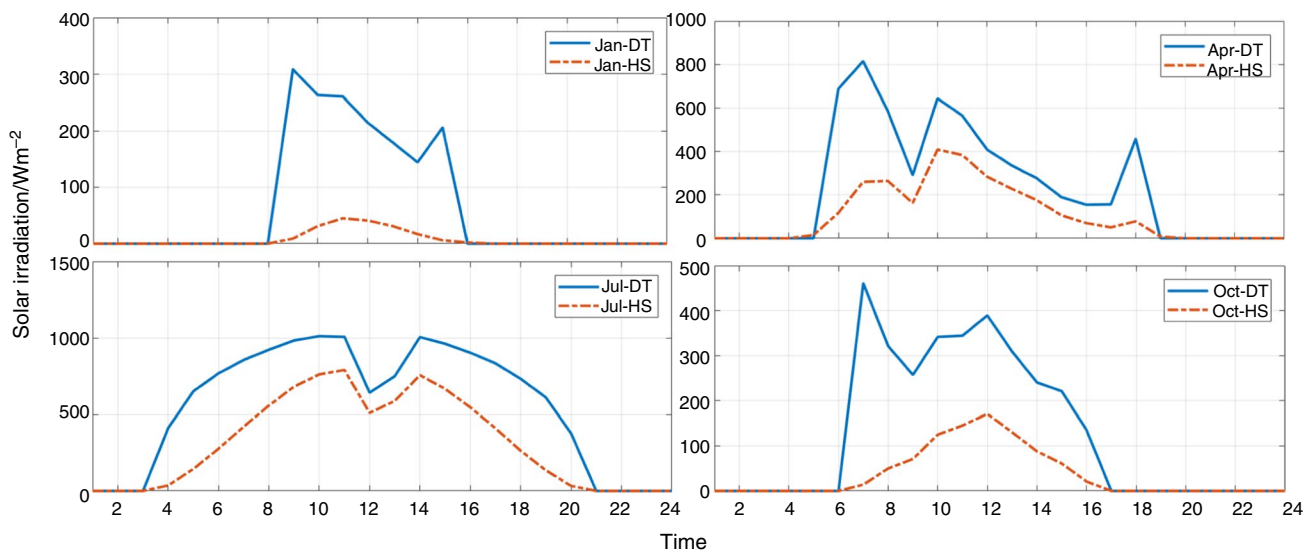


Fig. 4 Comparison of the amount of receivable solar energy by a fixed and a tracking collector

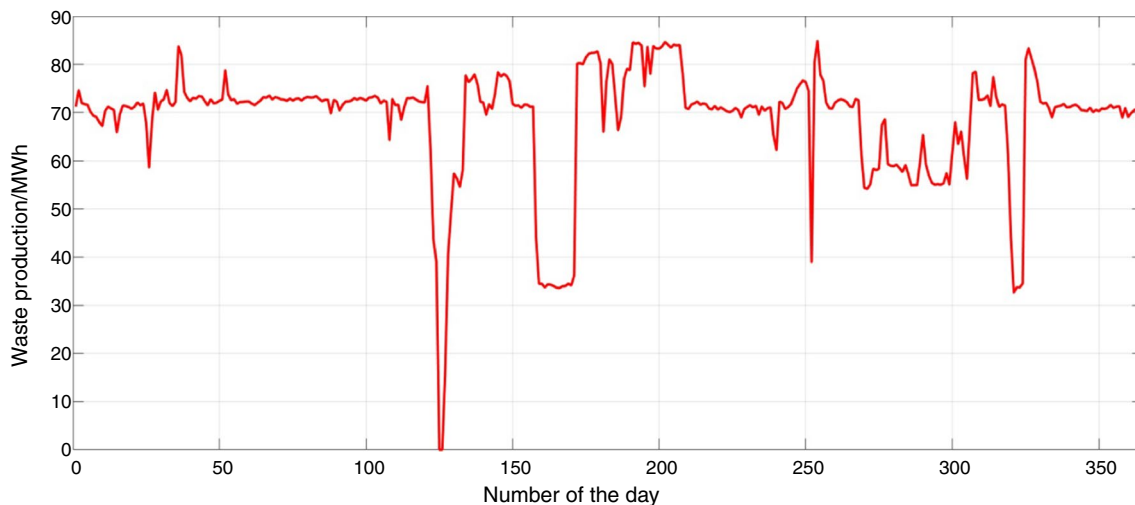


Fig. 5 Aarhus waste incineration capacity along the year 2015

Validation of the PTC model

Naturally, for making reliable results, the models used for the simulations should be validated. The models used for the Rankine cycle and waste incineration processes are validated in different ways in the literature. Here, however, the model used for the PTCs is validated. For this, the results are compared with the experimental results presented in [50]. Figure 6 makes this comparison for several different cases, i.e., different solar irradiation levels, temperatures, operating fluids, etc. According to the figure, a very good agreement between the referenced values and calculated values is seen. Here, the maximum and mean differences are only 0.1% and 0.06%, respectively.

Energy analysis results

Table 2 presents information about the physical properties of the working fluid in the Rankine cycle. As such, the last column of the table gives the mass flow rate of the working fluid at a different point along the cycle while working in the nominal load, just to be an indication of the share of the working fluids withdrawn for reheat and regenerations loops, etc.

For any power plant, there should be a pattern based on which the power plant bids for power sales. This bidding process, which should be done every day and takes place in the power market, requires complicated calculations and is out of the scope of this work. However, as a power-sale

Fig. 6 Validation of the parabolic trough model in comparison with the results given in [50]

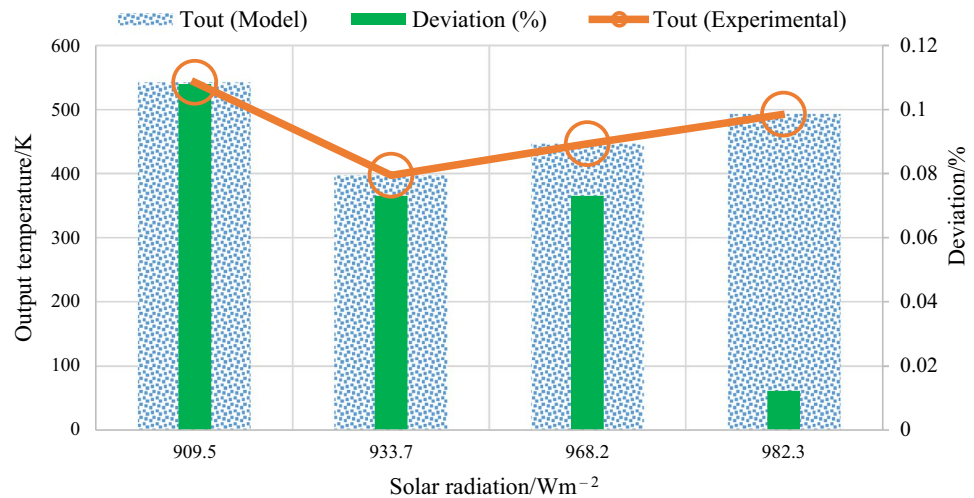


Table 2 Values of physical properties of the steam/water in different positions along the power block

Point	P/bar	T/K	$h/\text{kJ kg}^{-1}$	$s/\text{kJ kg}^{-1}\text{K}^{-1}$	$m'_{\text{nominal}} / \text{kg s}^{-1}$
1	100	773.2	3373.998	6.597	21.54
2	30	622.8	3113.855	6.741	21.54
3	30	773.2	3456.597	7.234	18.03
4	2.5	573	3069.846	7.787	2.18
5	0.1	318.9	2583.104	8.147	15.85
6	0.1	318.9	191.719	0.6489	15.85
7	2.5	319	192.042	0.6491	15.85
8	2.5	400.6	535.387	1.607	18.32
9	100	402.3	549.229	1.616	18.32
10	100	507	1007.241	2.643	18.32
11	30	507	1008.241	2.645	3.51
12	100	509.2	1019.564	2.651	3.51
13	100	487.6	920.7	2.453	21.54

pattern is required to be able to simulate the performance of the power plant, relying on the facts presented about the system characteristics and its operational restrictions, a daily power sales strategy is defined in this work. Based on this strategy, the power plant is committed to provide a uniform amount of $X + 5$ MW power during the day (from sunshine to sunset) and the uniform amount of 5 MW during the night, where X is the maximum instantaneous power which is producible by the incoming solar irradiation during a given day. The number 5 is the minimum allowed of waste incineration load. Figure 7 shows this parameter for the four typical seasonal days. As seen, the sales value is considerably higher during the summer as more solar energy is available. Naturally, when no solar irradiation is coming, e.g., winter days, the load of the power plant decreases as well.

As explained before, the power plant is supposed to have the nominal capacity of 20 MW and the solar field is so sized that it can support the required heat for producing 15 MWe by the Rankine cycle. The calculations show that a Rankine cycle with the characteristics given in Table 3 will offer a net efficiency of 34%. Thus, for producing 15 MWe power, the solar field should be sized for 44 MW of maximum heat output. Knowing the amount of energy obtainable from one single collector, similar to that characterized in Table 1, one could size the solar farm of the power plant. Figure 8 shows the amount of net heat produced by one set of LS2 PTCs for the four sample seasonal days. The observations reveal that a peak amount of 140 kW heat may be produced by each collector. Therefore, a total of 315 LS2 parabolic trough solar collectors are required for the sized solar–waste hybrid power plant of this work.

Figure 9 illustrates the effects of variation of the collectors' outlet temperature on the thermal efficiency of the collector as well as its net heat output. As seen in the figure, the efficiency and the rate of net heat output decrease as the collectors' outlet temperature increases and vice versa. Figure 9 shows that as the solar working fluid increases, the efficiency of the collector decreases. The reason is that the irreversibility increases due to the temperature increase of the working fluid and consequently increasing the temperature difference between the working fluid and the ambient. Two heat transfer factors lose heat from the pipe to the ambient, convective heat transfer between the cover and the ambient as well as radiative heat transfer between the cover and the sky. These two factors of heat loss increase as the working fluid temperature increases. The maximum thermal efficiency of 72% and net heat output of 180 kW are obtained for the low outlet temperature of 500 K while these two will decrease to, respectively, 32% and 80 kW if the fluid outlet temperature reaches 1000 K.

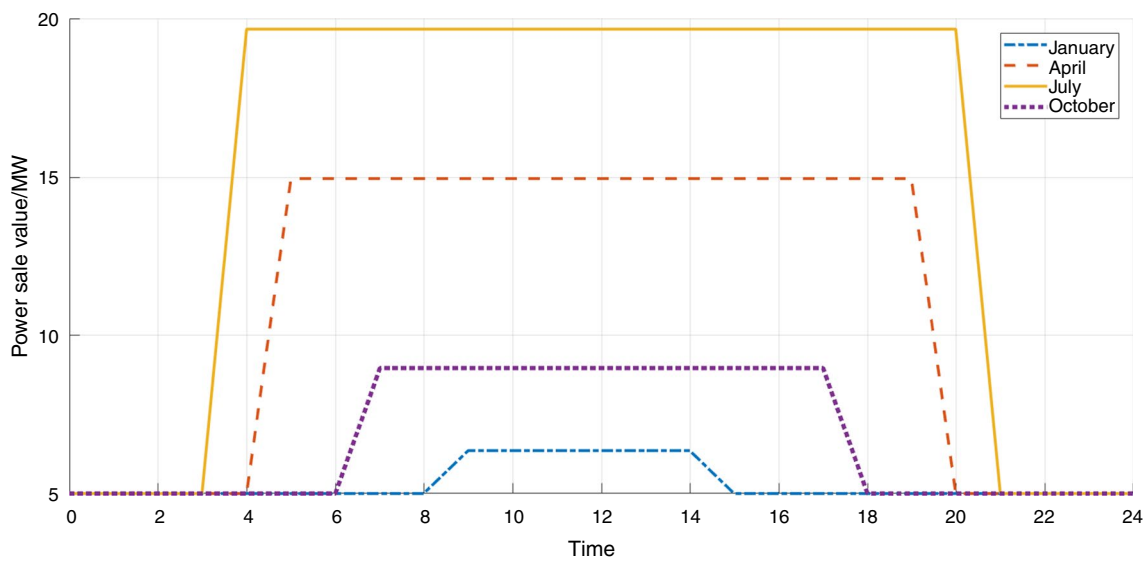


Fig. 7 Electricity sales plan of the hybrid power plant

Table 3 Exergy performance audit of the Rankine cycle components

Components	Exergy destruction/kW	Exergy Efficiency/%	Exergy destruction of the components relative to the cycle/%
Boiler	8462	64	36.00
Turbine	4892	67	20.80
Condenser	1244	86	5.30
Pump 1	0.6	77	0.01
Pump 2	23	81	0.10
Pump 3	2.9	86	0.01
OFWH	297.4	65	1.30
CFWH	8417	12	35.82
Chamber	162	93	6.90

Figure 10 shows the share of the solar thermal system and the waste incineration unit in the heat production of the hybrid power plant for the four sample days. This figure is based on the power sales strategy defined for the power plant. Naturally, during the nights, the solar thermal system contribution is zero and the waste incineration unit provides enough heat for producing 5 MW of power output (5 MW of power/0.34 as the efficiency of the cycle = 14.7 MW heat). During the day, on the other hand, the amount of power output of the cycle should be constant always. Thus, any reduction of solar energy availability should be compensated by a higher rate of heat output from the waste incinerator.

Figure 11 shows the trend of the energy efficiency of the hybrid power plant during the sample days. According to the figure, the maximum energy efficiency of the cycle is 27%, which is obtained when the waste incineration is

working at the full load and no solar heat is injected into the system. This value is indeed the result of the waste incineration process efficiency (80%) multiplied by the Rankine cycle thermal efficiency (34%). As seen, as the share of solar heat increases, the efficiency of the plant decreases and this is due to the low conversion efficiency of the PTC, which is a rational finding. One should note although the conversion efficiency of such solar collector is low, its effective role in hiring the free source of solar energy at a high temperature suitable for power production makes it an interesting technology and highly worthy of investment. From a practical point of view, it could be noted that about 11% of the required energy of this plant is provided from the free source of solar energy. This contribution increases the share of renewable energy in the chain of energy supply.

Figure 12 shows a duration curve of the energy efficiency of the hybrid cycle throughout the year. As can be seen, the maximum efficiency value of the plant will be 27.1% which is related to the cases when the share of the solar system is zero (100% supply from the waste incineration). This is, in fact, the dominant state of the power plant for about 68% of the year period. On the other hand, the lowest energy efficiency of the cycle will be when the contributions of the solar and waste incineration systems are, respectively, maximized (75%) and minimized (25%), which is equal to 19.5%. This, naturally, happens only a few times a year. About 2800 h a year the power plant efficiency will be between the maximum and minimum values as the solar share varies for these times.

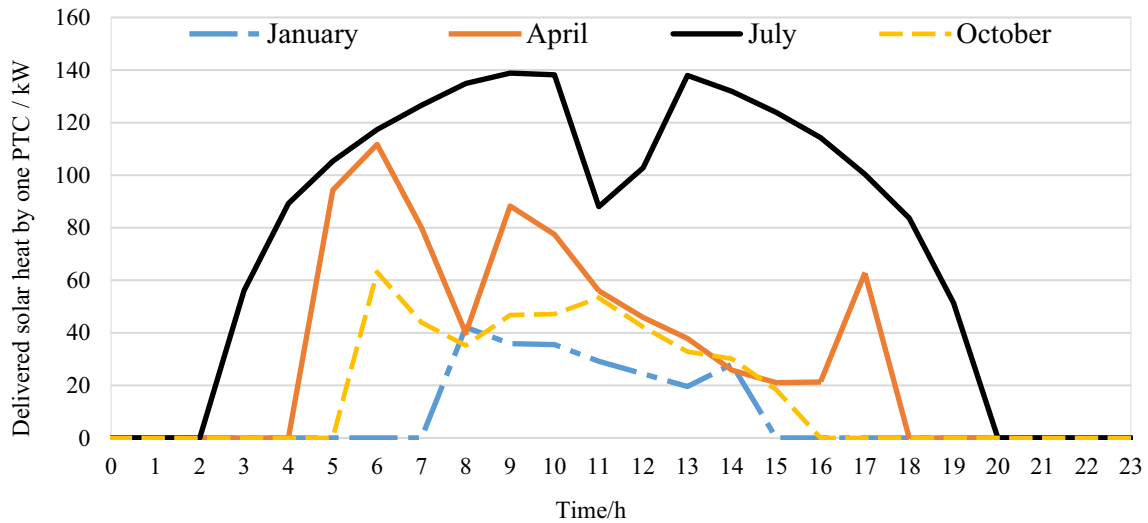


Fig. 8 The rate of net heat producible by a tracking LS2 PTC over the sample days

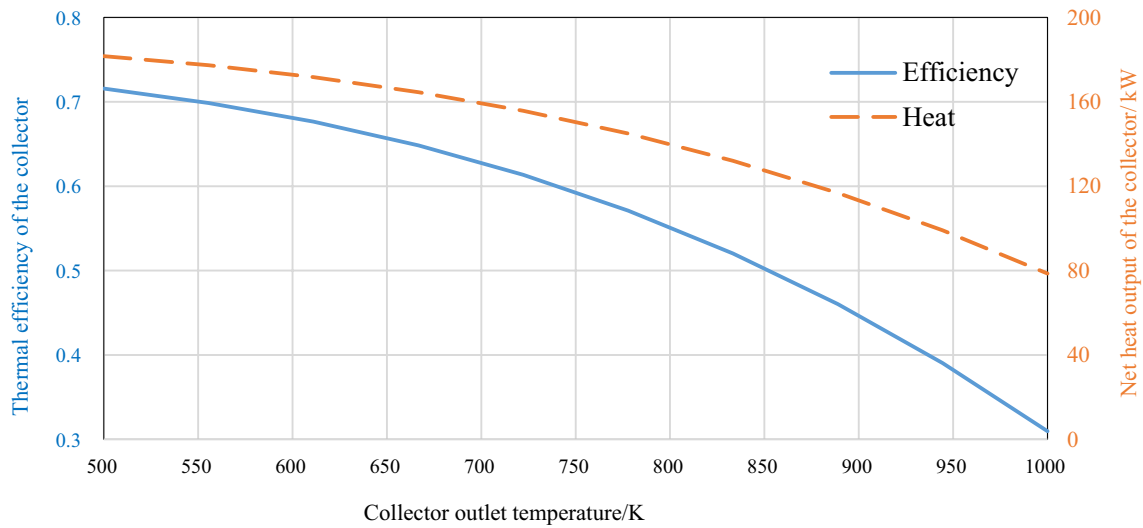


Fig. 9 Impact of outlet temperature of the fluid on the thermal efficiency and rate of heat output of the LS2 PTC

Fig. 10 Shares of the solar collector field and the waste incinerator in thermal energy preparation for the cycle

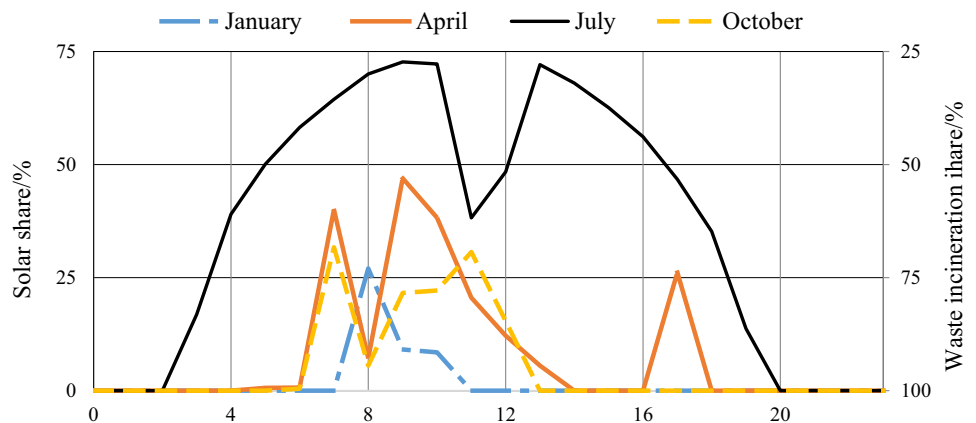


Fig. 11 Thermal efficiency of the combined solar–waste power plant during the four typical days

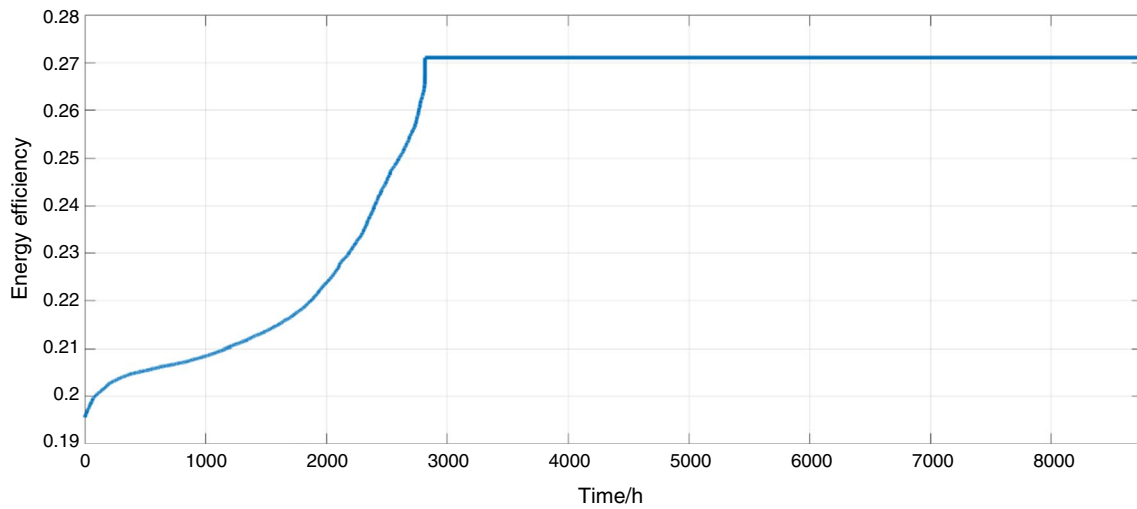
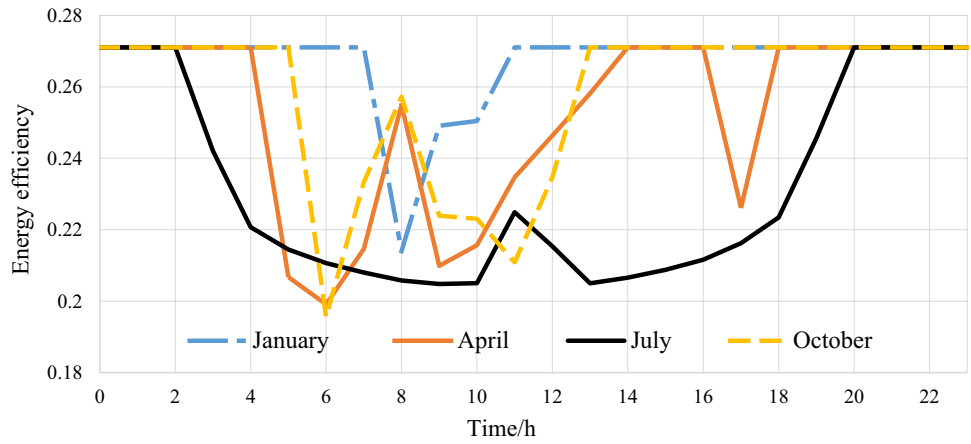


Fig. 12 The thermal efficiency of the combined solar–waste power plant throughout the year

Fig. 13 The collector exergy efficiency for various mass flow rates and inlet working fluid temperatures

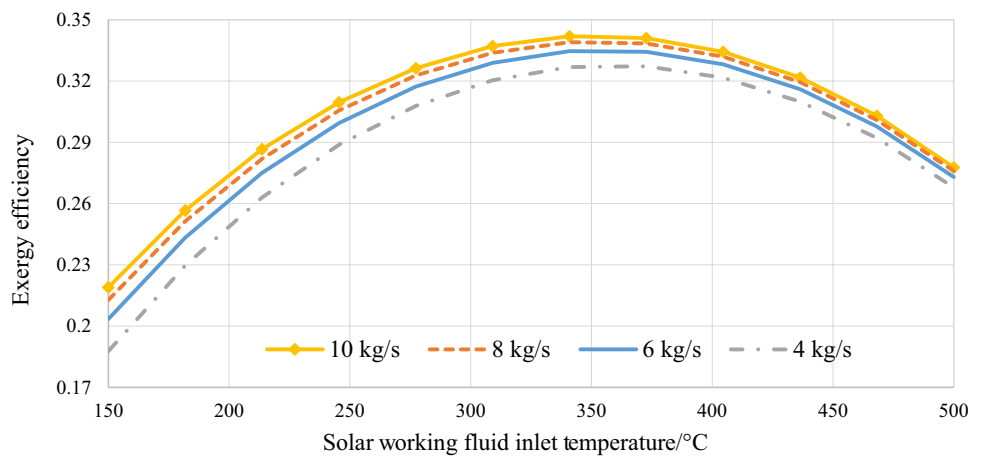
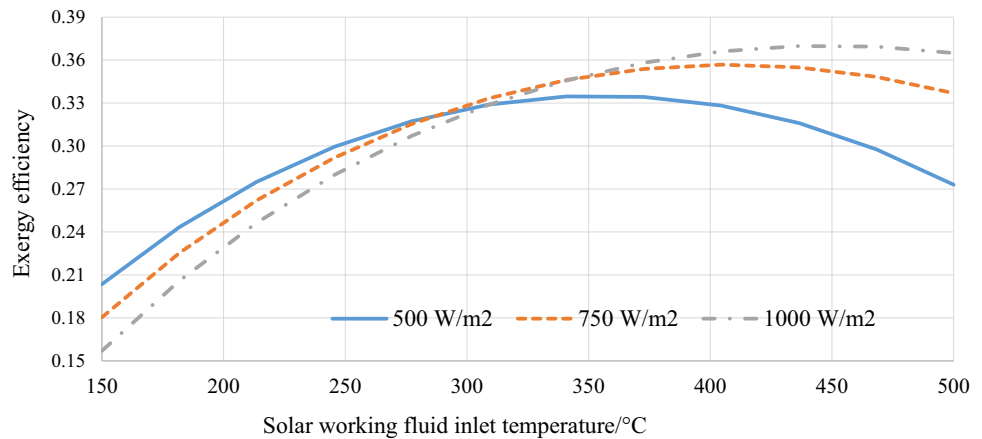


Fig. 14 The collector exergy efficiency for various solar irradiations and inlet working fluid temperatures



Exergy analysis results

For exergy analysis results, first of all, it is the exergy performance assessment of the LS2 PTC that is presented and discussed. Figure 13 shows the exergy efficiency of the collector in a wide range of inlet working fluid temperatures for various working mass flow rates. According to the figure, a higher mass flow rate results in a better exergy performance of the collector while, regardless of the mass flow rate, there is an extremum point for the optimal input fluid temperature, i.e., around 350 °C, resulting in the best exergy efficiency of the collector, i.e., around 33–34% for various considered mass flow rates.

Figure 14 investigates the effect of solar irradiation intensity on the exergy performance of the collector. Here also, a wide range of working fluid inlet temperatures are examined. It is seen that there is no stable trend for the variation of the exergy efficiency of the collector versus the variation of the solar irradiation, that is, in low inlet fluid temperatures, increasing the solar irradiation leads to the reduction of the exergy efficiency of the collector while after some point, i.e., 300 °C, the trend becomes inverse. From Figs. 13 and 14, it could be concluded that if one would extract the highest energy from the PTC, as much as possible, the Rankine cycle should be controlled so that the output temperature of the solar working fluid at the outlet of the boiler will be changed according to the amount of the solar radiation, e.g., when the solar radiation is about the 500 W m⁻² and 1000 W m⁻², the outlet temperature should be around the 350 °C and 450 °C, respectively.

Having this information about the effective parameters on the exergy performance of the LS2 PTCs, Fig. 15 shows the exergy gain of one single collector in the system. This comes for the entire year (up) and the 4 sample days for better illustration of the fluctuations (down). According to the figure, the maximum possible exergy input of the collector set is 15 kW which is naturally achieved during the times

with higher solar irradiation intensity. As the solar intensity falls, the exergy input of the collector also decreases.

Similarly, Fig. 16 shows the exergy efficiency of the collector module during the year (up) and the four typical seasonal days (down). It is observed that the exergy efficiency of the solar field does not exceed 0.37% at any point during the year. Here, it is seen that, during the sunnier days, better exergy efficiency of the plant is obtained; however, this cannot be generalized because the exergy efficiency, in addition to the solar irradiation intensity, is a function of ambient temperature and more importantly the inlet temperature of the solar working fluid. During the sample day of January, the exergy efficiency does not exceed the low value of 14%.

In the next step, one should assess the performance of the incineration process exergetically. Figure 17 shows the rates of input exergy and exergy destruction of the waste incineration unit for various loads of the incinerator. This includes the exergy destruction rate through Boiler 2 as well. Naturally, this starts from the minimum load of 5 MW as the incinerator is not going to work below 25% of its nominal load (20 MW). As seen, at full load, the input exergy of the waste incineration unit will be about 120 MW out of which, about 68 MW is destroyed. In the minimum load of 5 MW, the exergy destruction rate will be 17 MW while the input exergy is about 30 MW. Dividing these values to each other for the full and minimum loads, one can find out that the exergy efficiency of the system will be constant in all loads, i.e., 43%. Although this may not be realistic for dynamic operation conditions, this finding is yet correct in this work as this study neglects the effects of the partial load operation. Note that for the presented results so far, based on the advice coming from [36], the rate of excess air in the incineration process was considered 80%.

Figure 18 shows the rate of exergy destruction of various components of the Rankine cycle during the year. The figure is presented based on the duration curves to see in what portion of the time a year a component goes for its highest rate

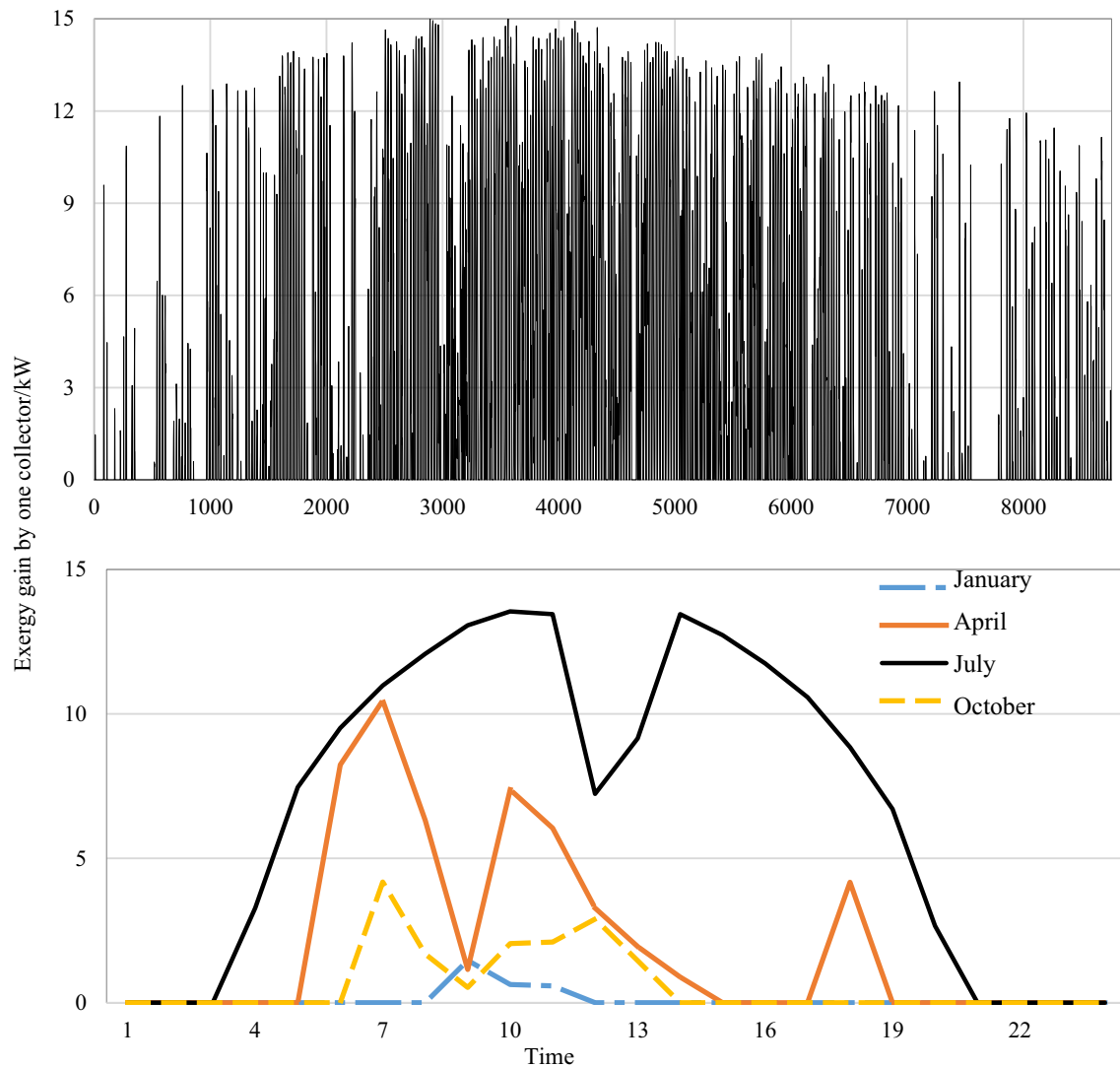


Fig. 15 The exergy gain of one LS2 PTC along the year and the 4 sample days

of irreversibility. As seen, the highest exergy losses occur in the closed feedwater tank and then, it is the steam generators (both Boilers 1 and 2) that cause the largest rates of irreversibilities. Expectedly, pumps and the mixing chamber do not make that amount of exergy destruction in the cycle.

Table 3 gives information about the exergy destruction rate of the components when working in full load. The table also presents information about the obtained exergy efficiency of the components. Note that here also as the effects of partial load operation are neglected, regardless of the type of heat source, a certain and constant exergy efficiency is obtained for the Rankine cycle which is 50%.

Having the presented information about the main subsystems of the hybrid power plant, i.e., the solar thermal unit, the waste incineration unit, and the Rankine cycle, one could make an assessment of the exergy performance of the whole hybrid power plant. Figure 19 presents information about

the hourly average rate of irreversibility in the entire power production complex. According to the figure, during the summer, the rate of irreversibilities in the system is higher. This is mainly due to the fact that during summer more solar energy is available, thus, the power sales strategy is based on more power sales values. Therefore, the rate of exergy destruction is also higher than in winter and fall.

In Fig. 19, it is seen that the exergy destruction rate at the nominal load operation of the hybrid system is about 110 MW. As the exergy output of the system in this condition is only 20 MW (equal to the power output of the system), therefore, the exergy efficiency of the system should be rather small. Figure 20 shows the duration curve of the hourly averaged exergy efficiency of the hybrid power plant. Confirming the finding of the previous figures, an exergy efficiency not better than 21.5% is achieved from the hybrid power plant. Just taking the previous figures into account,

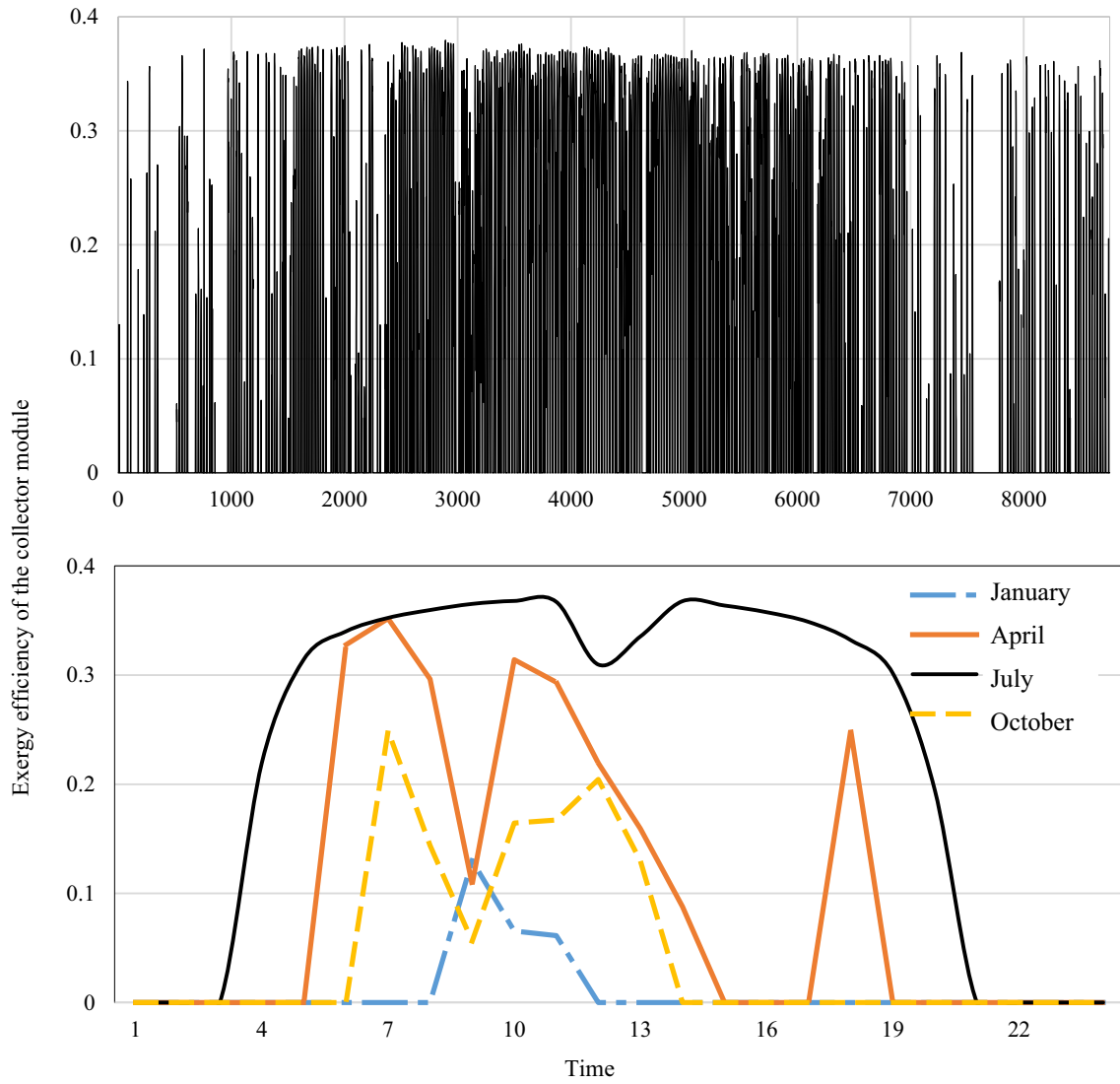
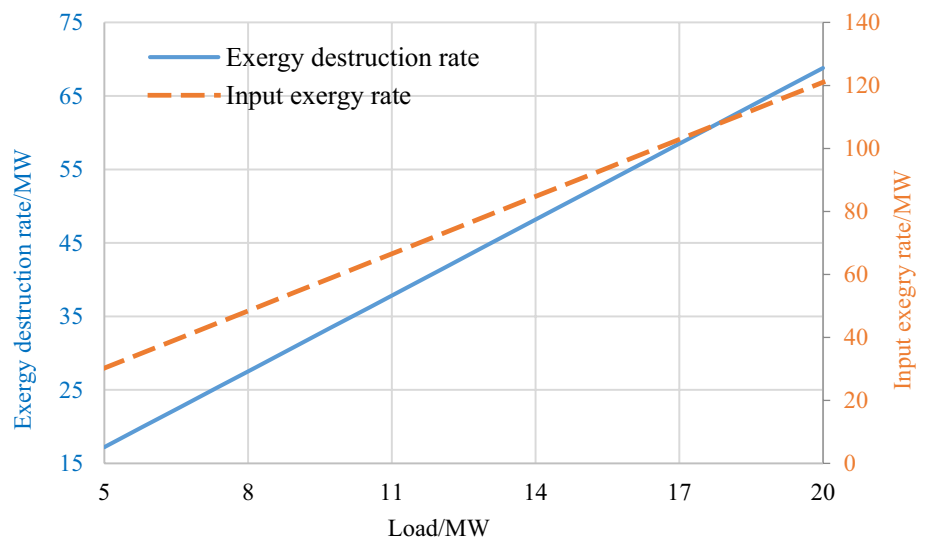


Fig. 16 The exergy efficiency of the solar farm along the year and the 4 sample days

Fig. 17 The rate of exergy destruction and input exergy of the incinerator in various operating loads



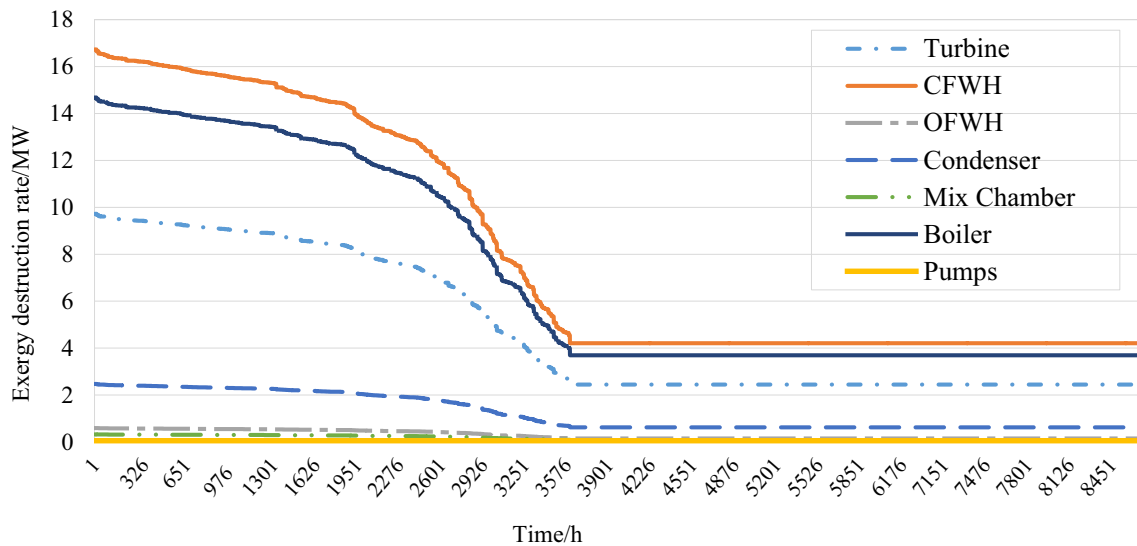


Fig. 18 Duration curve of exergy destruction rate in different components in the Rankine cycle

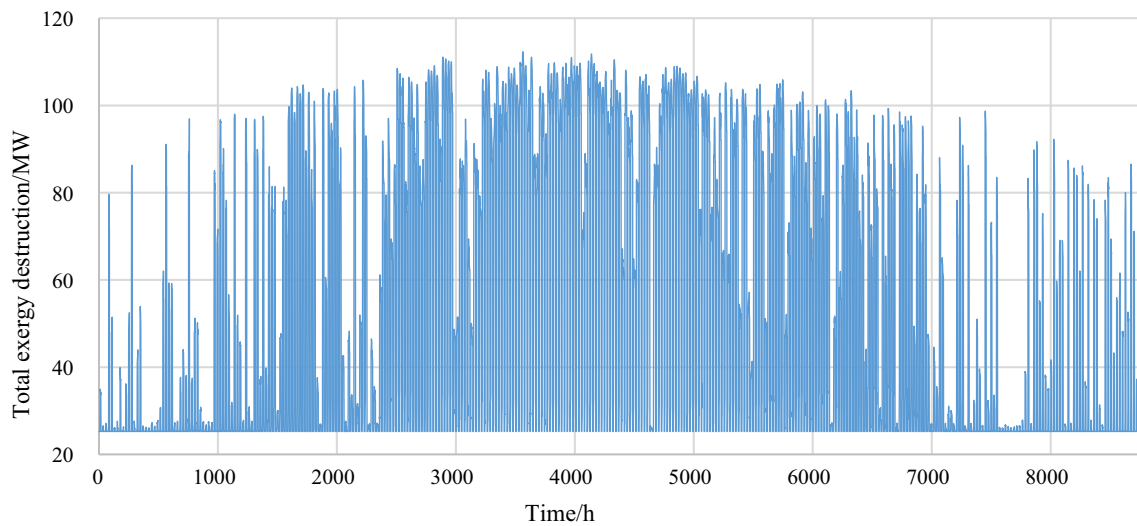


Fig. 19 Rate of irreversibility for the entire cycle throughout the year

one may easily rank the exergy destruction sources in the power plant. It will be the solar field that makes the largest irreversibilities. Then, the waste incinerator causes the second largest value of exergy destruction in the system. The turbine set is another source that makes a huge rate of exergy destruction in the Rankine cycle.

Figure 21 accomplishes a sensitivity analysis of the exergy efficiency of the hybrid cycle for various shares of solar and waste incineration boilers. This would help to better understand the role of the incineration process and the solar thermal systems in the exergy performance of the hybrid power plant. The figure includes the share of waste

incineration from 25% (minimum possible share) up to 100% (full-load operation of the cycle with waste source only). On the other hand, the share of solar energy can be between 0% (when no solar energy is available) and 75% (when maximum solar irradiation comes to the solar farm). Overall, maximum exergy efficiency of about 22% (at full waste incineration load) and a minimum of just above 17% (when the solar share is at an average level) are achievable from the hybrid system. The interesting finding is that there is the worst share of solar energy for the system exergetically. That is the solar share of 40% before and after which the exergy efficiency of the cycle increases.

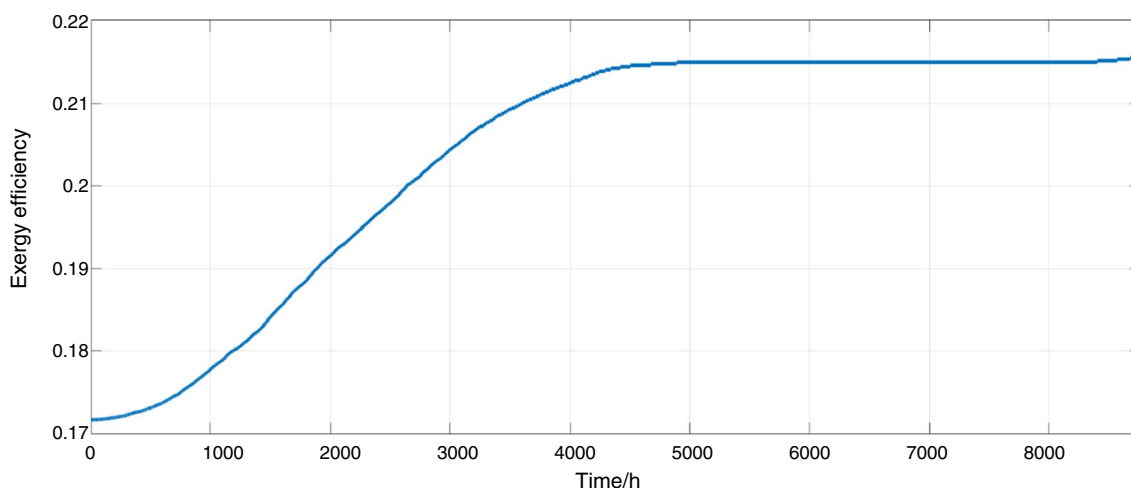


Fig. 20 Duration curve of the exergy efficiency of the hybrid cycle along the year

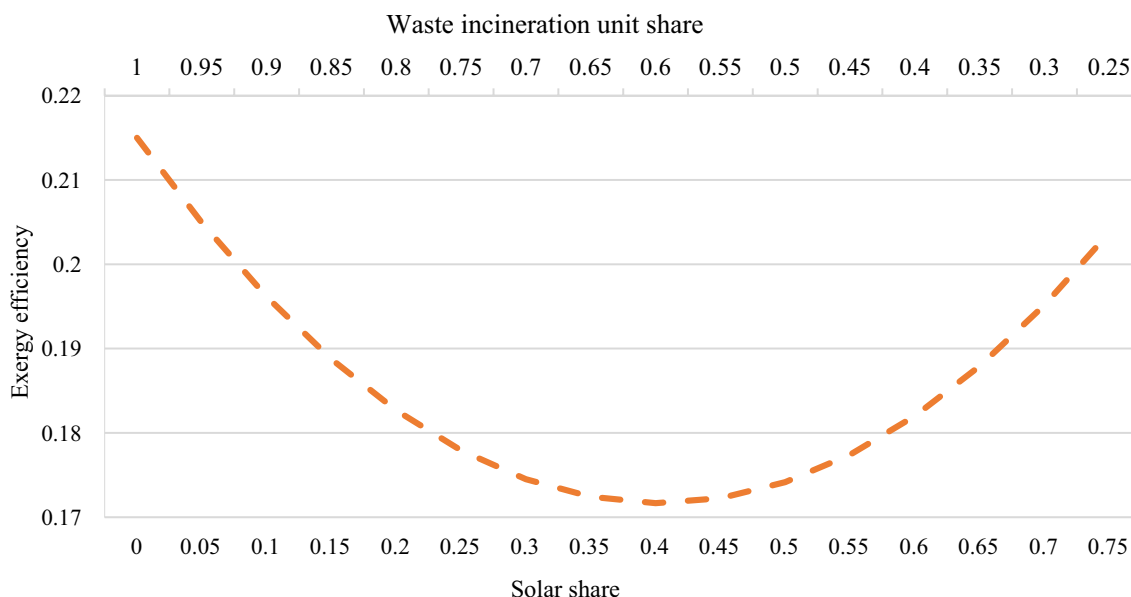


Fig. 21 Sensitivity analysis of the exergy efficiency of the cycle for various shares of solar and waste incineration boilers

LCOE and emission

Figure 22 compares the total hourly emission of the hybrid plant with that of a power plant driven by a waste incinerator only (i.e., no solar energy for the same power sales pattern). This figure helps to perceive the role of the solar thermal system for making the system more environmentally friendly. Clearly, the level of emission reduction is much larger during the summer when more solar energy is available.

The next step is to compare the amount of emission of the hybrid power plant with those of regular power production systems, e.g., natural gas-driven Rankine power plant and

gas turbine. To make a fair judgment, in this comparison, the absolute environmental impact of our hybrid power plant is taken into account. This, indeed, means considering both the emission that our plant is causing and the emission that is prevented by burning the municipal waste rather than simply landfilling of the waste. According to [47], municipal waste landfilling causes an average of 840 kg of CO₂e per tonne of waste while incineration of the same amount of waste would make only 415 tonnes of CO₂e. Thus, incineration of municipal waste is indeed a way of preventing a further amount of emission, i.e., 425 kg CO₂e per tonne of waste. By this information, Fig. 23 compares the combined solar–waste power plant, a conventional natural gas-driven

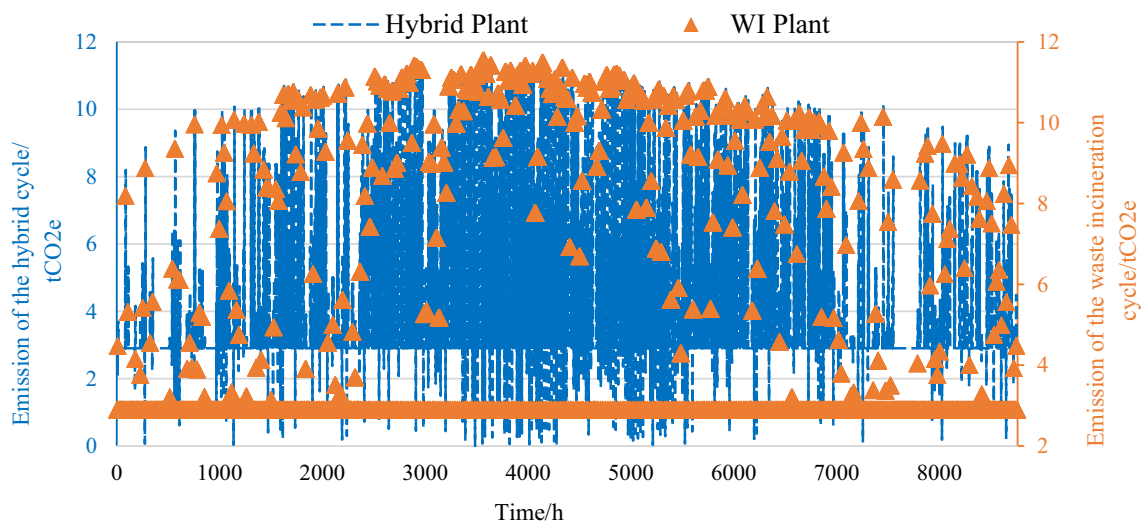


Fig. 22 Comparison of the hourly equivalent CO₂ emission of the hybrid system with a waste incineration plant

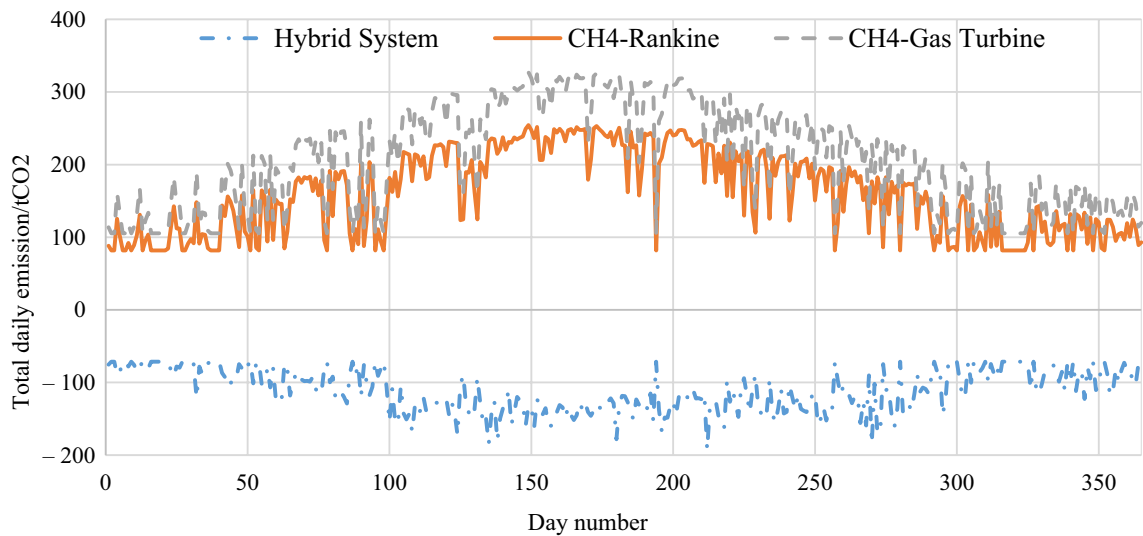


Fig. 23 Total daily effective equivalent CO₂ emission of the hybrid system compared to a natural gas-fired Rankine cycle and a gas turbine

Rankine cycle, and a conventional gas turbine in terms of environmental impacts. According to the figure, there is a big difference between the environmental impacts of the power plants. The negative level of released greenhouse gases means much environmental benefit via preventing pollutants being released to the environment in the combined solar–waste plant while the others cause a significant quantity of pollution released to the environment.

In the end, Fig. 24 compares the LCOE of the hybrid power plant with some other popular and conventional power production technologies. The figure considers the share of four types of costs in the total LCOE of the system, e.g., capital investment, fixed and variable operation and maintenance costs, and

fuel costs. Naturally, as the system is complex and intelligently designed, presenting interesting services compared to the other systems, it should not be expected that the system outperforms the other systems in terms of the LCOE value as well. However, as the figure shows, the LCOE of the system is still very close to the others. The main reason for this is the free source of energy in the hybrid system, i.e., waste/solar energy, while for the conventional systems, e.g., biomass and gas plants, a huge portion of the LCOE is related to the cost of fuel. Among the considered cases, wind power and solar PV offer lower LCOE values both of which suffer from fluctuating power output. The gas combined cycle and waste incineration plants also offer interesting LCOE values but the main problem with

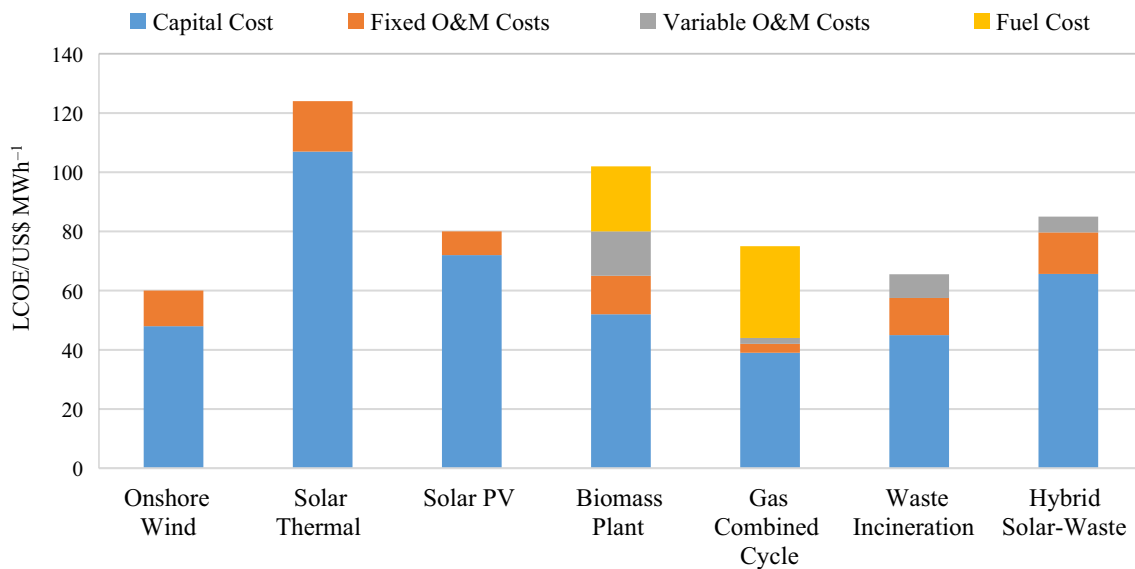


Fig. 24 Comparison of the LCOE of the plant with some power plant technologies

these systems is their emission. It is noteworthy that, this study does not take emission taxes into consideration. If emission taxes come into account as well, the LCOE of the hybrid cycle would even be more interesting.

Conclusions

This work presents a thorough thermodynamic and sustainability analysis (comprising energy, exergy, economic and environmental analyses) of a hybrid Rankine-based power production system in which the driving heat is provided by a combination of PTCs and a waste incinerator. This novel hybrid renewable power plant will contribute to a higher share of renewables in the future energy systems due to the several advantages it offers from energy, cost and environmental points of view. This is evident that renewable energies improve energy security in a long run and reduce dependence on fossil resources. This means having access to the requisite volumes of energy at affordable prices. Solar energy as a sustainable energy source, when combined with an agile energy output stabilizer as a waste incinerator, for electricity generation can significantly increase the energy security level. Consequently, this hybrid system not only enhances energy security but also decreases the environmental concerns about waste production.

The results of the energy analysis showed that the system offers the annual average thermal efficiency of 25% which is an interesting value for a system with solar concentrating units. The exergy efficiency of the system is, however, not that satisfactory, only about 20%, due to the large exergy

destructions mainly in the solar farm, the incinerator, and the turbine set of the Rankine cycle. A simple method of improving this factor is to revise the preheating process of the feedwater before the first boiler. Also, an optimal operation strategy based on which the solar system and the waste incineration unit could perform better exergetically can remarkably be beneficial for this objective. The results of environmental impact analysis show that the hybrid system not only outperforms all other conventional power production systems, but also prevents a huge amount of greenhouse gases being emitted via incineration of municipal waste instead of landfilling. The economic assessment calculates the LCOE of the hybrid solar–waste Rankine-based system, 82 USD MWh⁻¹, which is more or less in the same range as others, proving the excellence of the proposal taking the supreme energy, exergy and environmental performance of the system.

Based on the definitions, sustainability stands on the three main pillars of economic, social and environmental aspects. The investigated system of this work is considered a sustainable solution because:

1. environmentally speaking, it leads to massive amount of emission reduction;
2. economically speaking, its LCOE is much inspiring and even comparable with the LCOE of wind turbines and PV plants;
3. and socially speaking, it paves the path for a cleaner and healthier environment as well as access to cheap and reliable energy in electricity sector.

References

- Plis A, Kotyczka-Morańska M, Kopczyński M, Łabojko G. Furniture wood waste as a potential renewable energy source. *J Therm Anal Calorim.* 2016;125:1357–71.
- Senturk Acar M, Arslan O. Energy and exergy analysis of solar energy-integrated, geothermal energy-powered Organic Rankine Cycle. *J Therm Anal Calorim.* 2019;137:659–66.
- Peng Y, Zahedastjerdi A, Abdollahi A, Amindoust A, Bahrami M, Karimipour A, et al. Investigation of energy performance in a U-shaped evacuated solar tube collector using oxide added nanoparticles through the emitter, absorber and transmittal environments via discrete ordinates radiation method. *J Therm Anal Calorim.* 2019;20:1–9.
- Jeon J, Lee J-H, Seo J, Jeong S-G, Kim S. Erratum to: application of PCM thermal energy storage system to reduce building energy consumption. *J Therm Anal Calorim.* 2014;116:539.
- Guerrero-Lemus R, Martínez-Duart JM. Renewable energies and CO₂: cost analysis, environmental impacts and technological trends—2012 edition. In: Guerrero-Lemus R, Martínez-Duart JM, editors. London: Springer; 2013. p. 307–33.
- Mousavi GSM, Faraji F, Majazi A, Al-Haddad K. A comprehensive review of Flywheel Energy Storage System technology. *Renew Sustain Energy Rev.* 2017;67:477–90.
- Rehman S, Al-Hadhrani LM, Alam MM. Pumped hydro energy storage system: a technological review. *Renew Sustain Energy Rev.* 2015;44:586–98.
- Arabkoohsar A, Andresen GBB. Design and analysis of the novel concept of high temperature heat and power storage. *Energy.* 2017;126:21–33. <https://doi.org/10.1016/j.energy.2017.03.001>.
- Bagherzadeh SA, Ruhani B, Namar MM, Alamian R, Rostami S. Compression ratio energy and exergy analysis of a developed Brayton-based power cycle employing CAES and ORC. *J Therm Anal Calorim.* 2020;139:2781–90.
- Nouri M, Namar MM, Jahanian O. Analysis of a developed Brayton cycled CHP system using ORC and CAES based on first and second law of thermodynamics. *J Therm Anal Calorim.* 2019;135:1743–52.
- Romanelli F. Strategies for the integration of intermittent renewable energy sources in the electrical system. *Eur Phys J Plus.* 2016;131:53.
- Akbari Vakilabadi M, Bidi M, Najafi AF, Ahmadi MH. Energy, Exergy analysis and performance evaluation of a vacuum evaporator for solar thermal power plant zero liquid discharge systems. *J Therm Anal Calorim.* 2019;20:1–6.
- Achour L, Bouharkat M, Behar O. Performance assessment of an integrated solar combined cycle in the southern of Algeria. *Energy Rep.* 2018;4:207–17.
- Liu T, Liu Q, Wang X, Sui J, Jin H. Performance investigation of a new solar-hybrid fuel-fired distributed energy system integrated with a thermochemical process. *Energy Procedia.* 2017;142:815–21.
- Pärisch P, Mercker O, Warmuth J, Tepe R, Bertram E, Rockendorf G. Investigations and model validation of a ground-coupled heat pump for the combination with solar collectors. *Appl Therm Eng.* 2014;62:375–81.
- Basir Khan MR, Jidin R, Pasupuleti J, Shaaya SA. Optimal combination of solar, wind, micro-hydro and diesel systems based on actual seasonal load profiles for a resort island in the South China Sea. *Energy.* 2015;82:80–97.
- Li P, Li J, Pei G, Munir A, Ji J. A cascade organic Rankine cycle power generation system using hybrid solar energy and liquefied natural gas. *Sol Energy.* 2016;127:136–46.
- Kasaeian A, Nouri G, Ranjbaran P, Wen D. Solar collectors and photovoltaics as combined heat and power systems: a critical review. *Energy Convers Manag.* 2018;156:688–705.
- Haddad A, Ramadan M, Khaled M, Ramadan H, Becherif M. Study of hybrid energy system coupling fuel cell, solar thermal system and photovoltaic cell. *Int J Hydrogen Energy.* 2018 (in press). <https://doi.org/10.1016/j.ijhydene.2018.06.019>.
- Arabkoohsar A, Andresen GBB. Supporting district heating and cooling networks with a bifunctional solar assisted absorption chiller. *Energy Convers Manag.* 2017;148:184–96.
- Liu M, Steven Tay NH, Bell S, Belusko M, Jacob R, Will G, et al. Review on concentrating solar power plants and new developments in high temperature thermal energy storage technologies. *Renew Sustain Energy Rev.* 2016;53:1411–32.
- Cavallaro F, Zavadskas EK, Streimikiene D. Concentrated solar power (CSP) hybridized systems. Ranking based on an intuitionistic fuzzy multi-criteria algorithm. *J Clean Prod.* 2018;179:407–16.
- McTigue JD, Castro J, Mungas G, Kramer N, King J, Turchi C, et al. Hybridizing a geothermal power plant with concentrating solar power and thermal storage to increase power generation and dispatchability. *Appl Energy.* 2018;228:1837–52.
- Jin HG, Hong H. 12—Hybridization of concentrating solar power (CSP) with fossil fuel power plants. In: Lovegrove K, Stein WBT-CSPT, editors. Woodhead Publishing Series Energy. Sawston: Woodhead Publishing; 2012.
- Behar O. Solar thermal power plants—a review of configurations and performance comparison. *Renew Sustain Energy Rev.* 2018;92:608–27.
- Arvelakis S, Frandsen FJ, Dam-Johansen K. Determining the melting behaviour of ashes from incineration plants via thermal analysis. *J Therm Anal Calorim.* 2003;72:1005–17.
- Łach M, Mikuła J, Hebda M. Thermal analysis of the by-products of waste combustion. *J Therm Anal Calorim.* 2016;125:1035–45.
- European Commission. The role of waste-to-energy in the circular economy. Commun From Comm To Eur Parliam Counc Eur Econ Soc Comm Comm Reg [Internet]. 2017;11. <https://ec.europa.eu/environment/waste/waste-to-energy.pdf>.
- Münster M, Meibom P. Optimization of use of waste in the future energy system. *Energy.* 2011;36:1612–22.
- Eriksson O, Finnveden G, Ekvall T, Björklund A. Life cycle assessment of fuels for district heating: a comparison of waste incineration, biomass- and natural gas combustion. *Energy Policy.* 2007;35:1346–62.
- Udono K, Sitte R. Modeling seawater desalination powered by waste incineration using a dynamic systems approach. *Desalination.* 2008;229:302–17.
- Hedberg E, Project D. Potential for Absorption Cooling Generated from Municipal Solid Waste in Bangkok, Degree Project, Department of Management and Engineering, Linköpings University.
- Sadi M, Arabkoohsar A. Modelling and analysis of a hybrid solar concentrating-waste incineration power plant. *J Clean Prod.* 2019;216:570–84.
- Arabkoohsar A, Sadi M. A hybrid solar concentrating-waste incineration power plant for cost-effective and dispatchable renewable energy production. In: 2018 IEEE 7th International Conference Power Energy, PECon 2018; 2019.
- Dickes R, Lemort V, Quoilin S. Semi-empirical correlation to model heat losses along solar parabolic trough collectors; 2015, 28th international conference on efficiency, cost, optimization, simulation and environmental impact of energy systems, Pau, France.
- Jack TA, Oko COC. Exergy and exergoeconomic analysis of a municipal waste-to-energy steam reheat power plant for Port Harcourt city. *Int J Ambient Energy.* 2018;39:352–9.

37. Song G, Shen L, Xiao J. Estimating specific chemical exergy of biomass from basic analysis data. *Ind Eng Chem Res.* 2011;50:9758–66.
38. Dudley VE, Kolb GJ, Mahoney AR, Mancini TR, Matthews CW, Sloan M, et al. Test results: SEGS LS-2 solar collector. Sandia Natl. Lab.; 1994.
39. Arabkoohsar A, Andresen GB. Thermodynamics and economic performance comparison of three high-temperature hot rock cavern based energy storage concepts. *Energy.* 2017;132:12–21.
40. Incropera FP, Bergman TL, Lavine AS, DeWitt DP. Fundamentals of heat and mass transfer, 8th Edition, ISBN: ES8-1-119-32042-5, [Internet]. Wiley. 2018. <https://www.wiley.com/en-us/Fundamentals+of+Heat+and+Mass+Transfer%2C+8th+Edition-p-ES81119320425>.
41. Touloukian YS, DeWitt DP. Thermal radiative properties. Non-metallic solids; 1972. NASA, United States.
42. Yang H-C, Lee S-Y, Choi Y-C, Yang I-H, Chung DY. Thermokinetic analysis of spent ion-exchange resins for the optimization of carbonization reactor condition. *J Therm Anal Calorim.* 2017;127:587–95.
43. Javadi MA, Hoseinzadeh S, Ghasemiasl R, Heyns PS, Chamkha AJ. Sensitivity analysis of combined cycle parameters on exergy, economic, and environmental of a power plant. *J Therm Anal Calorim.* 2020;139:519–25.
44. Petela K, Szlek A. Energy and exergy analysis of solar heat driven chiller under wide system boundary conditions. *Energy.* 2019;168:440–9.
45. Padilla RV, Fontalvo A, Demirkaya G, Martinez A, Quiroga AG. Exergy analysis of parabolic trough solar receiver. *Appl Therm Eng.* 2014;67:579–86.
46. Carneiro MLNM, Gomes MSP. Energy, exergy, environmental and economic analysis of hybrid waste-to-energy plants. *Energy Convers Manag.* 2019;179:397–417.
47. US Environmental Protection Agency (USEPA) [Internet]. https://www.wbdg.org/FFC/EPA/EPACRIT/epa625_6_89_021.pdf.
48. Johnke B, Hoppaus R, Lee E, Irving B, Martinsen TMK. Good practice guidance and uncertainty management in national greenhouse gas inventories. 2000. Intergovernmental Panel on Climate Change.
49. Arabkoohsar A, Andresen GB. A smart combination of a solar assisted absorption chiller and a power productive gas expansion unit for cogeneration of power and cooling. *Renew Energy.* 2018;115:489–500.
50. Dudley V, Kolb G, Sloan M and KD. SEGS LS2 Solar Collector-Test Results. Rep. Sandia Natl. Lab. SSAN94-1884; 1996.

Publisher's Note Springer Nature remains neutral with regard to jurisdictional claims in published maps and institutional affiliations.